AD-A039 213 BELL AEROSPACE TEXTRON BUFFALO N Y F/G 20/4
NUMERICAL SOLUTION OF COMPLETE FLOWS AROUND EXTERNAL STORES.(U)
DEC 76 Z POPINSKI, W L RUSHMORE, S W ZELAZNY F44620-75-C-0003
UNCLASSIFIED 9236-927001 AFOSR-TR-77-0621 NL

| OF |
AD A039213

END

DATE FILMED
5-77

AFOSR - TR - 77 - 0621

ADA039213

# NUMERICAL SOLUTION OF COMPLETE FLOWS AROUND EXTERNAL STORES

December 1976

Approved for public release;
distribution unlimited.

Z. POPINSKI
W. L. RUSHMORE
S. W. ZELAZNY

DDC
RECEIVED
MAY 10 1977
D

FOR

DEPARTMENT OF THE AIR FORCE
AIR FORCE OFFICE OF SCIENTIFIC RESEARCH (AFSC)
BOLLING AIR FORCE BASE, DC 20332

F44620-75-C-0003

AD No.
DDC FILE COPY

Bell Aerospace TEXTRON
Division of Textron Inc.

AIR FORCE OFFICE OF SCIENTIFIC RESEARCH (AFSC)
NOTICE OF TRANSMITTAL TO DDC
This technical report has been reviewed and is
approved for public release IAW AFR 190-12 (7b).
Distribution is unlimited.
A. D. BLOSE
Technical Information Officer

Unclassified

SECURITY CLASSIFICATION OF THIS PAGE (When Data Entered)

| REPORT DOCUMENTATION PAGE | READ INSTRUCTIONS BEFORE COMPLETING FORM |
|---|---|
| 1. REPORT NUMBER: AFOSR - TR - 77 - 0621 | 2. GOVT ACCESSION NO. 3. RECIPIENT'S CATALOG NUMBER |
| 4. TITLE (and Subtitle): Numerical Solution of Complete Flows Around External Stores | 5. TYPE OF REPORT & PERIOD COVERED: Final Report, Aug 1974 — Dec 1976 |
| | 6. PERFORMING ORG. REPORT NUMBER: 9236-927001 |
| 7. AUTHOR(s): Z. Popinski, W. L. Rushmore, S. W. Zelazny | 8. CONTRACT OR GRANT NUMBER(s): F44620-75-C-0003 |
| 9. PERFORMING ORGANIZATION NAME AND ADDRESS: Bell Aerospace Textron, Division of Textron Inc., P. O. Box One, Buffalo, New York 14240 | 10. PROGRAM ELEMENT, PROJECT, TASK AREA & WORK UNIT NUMBERS |
| 11. CONTROLLING OFFICE NAME AND ADDRESS: Department of the Air Force, Air Force Office of Scientific Research, Bolling Air Force Base, DC 20332 | 12. REPORT DATE: Dec 1976; 13. NUMBER OF PAGES: 61 |
| 14. MONITORING AGENCY NAME & ADDRESS(if different from Controlling Office): 72p. | 15. SECURITY CLASS. (of this report): Unclassified; 15a. DECLASSIFICATION/DOWNGRADING SCHEDULE: N/A |

16. DISTRIBUTION STATEMENT (of this Report)

Reproduction in whole or in part is permitted for any purpose of the US Government.

DISTRIBUTION STATEMENT A
Approved for public release;
Distribution Unlimited

17. DISTRIBUTION STATEMENT (of the abstract entered in Block 20, if different from Report)

Same as (16) above

18. SUPPLEMENTARY NOTES

19. KEY WORDS (Continue on reverse side if necessary and identify by block number)

| | | |
|---|---|---|
| External Stores | Computer Programs | Functions |
| Sphere-Cone | Mathematical Models | |
| Flow Field | Separation | |
| Viscous Flow | Navier-Stokes Equations | |
| Finite Elements | Natural Coordinates | |

20. ABSTRACT (Continue on reverse side if necessary and identify by block number)

A computer code, based on a finite element algorithm, was developed to solve the governing equations for a three-dimensional flow around a spherically blunted cone at an angle of attack. The solution is valid for a boundary layer region, including the flow separation in the cross-flow direction in the leeward area. The required initial and boundary conditions for this solution are obtained from a finite difference computer program for laminar → next page

DD FORM 1 JAN 73 1473 EDITION OF 1 NOV 65 IS OBSOLETE

Unclassified

SECURITY CLASSIFICATION OF THIS PAGE (When Data Entered)

408855

20. ABSTRACT (continued)

compressible three-dimensional boundary layer flow. Extension of the analysis to include the turbulent transport using the mixing length theory and a two-equation turbulence model is described. The results demonstrate the capability of the finite element method to predict the three-dimensional boundary region flow with cross-flow separation in the leeward area and to model the effects of turbulent flow.

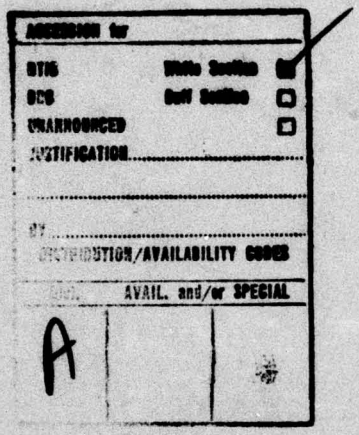


## ABSTRACT

A computer code, based on a finite element algorithm, was developed to solve the governing equations for a three-dimensional flow around a spherically blunted cone at an angle of attack. The solution is valid for a boundary layer region, including the flow separation in the cross-flow direction in the leeward area. The required initial and boundary conditions for this solution are obtained from a finite difference computer program for laminar compressible three-dimensional boundary layer flow. Extension of the analysis to include the turbulent transport using the mixing length theory and a two-equation turbulence model is described. The results demonstrate the capability of the finite element method to predict the three-dimensional boundary region flow with cross-flow separation in the leeward area.

TABLE OF CONTENTS


| | | Page |
|---|---|---|
| 1.0 | SUMMARY | 1 |
| 2.0 | INTRODUCTION | 2 |
| | 2.1 Background | 2 |
| | 2.2 Objectives and Approach | 6 |
| 3.0 | ANALYSIS | 12 |
| | 3.1 Governing Equations | 12 |
| | 3.2 Solution of the Forebody Flow Field | 17 |
| | 3.3 Initial and Boundary Conditions | 20 |
| | 3.4 Turbulence Models | 29 |
| | 3.4.1 Background | 29 |
| | 3.4.2 Approach | 30 |
| 4.0 | RESULTS AND FUTURE PLANS | 33 |
| | 4.1 Check Cases | 33 |
| | 4.2 Demonstration Cases | 36 |
| 5.0 | CONCLUSIONS | 45 |
| 6.0 | REFERENCES | 46 |
| APPENDICES | | |
| | A. Order of Magnitude Analysis | 49 |
| | B. Finite Element Formulation and Solution | 51 |
| | C. Solution of the Continuity Equation | 61 |

## ILLUSTRATIONS


| Figure | | Page |
|---|---|---|
| 2-1 | Separation Bubble Flowfield Model for Three-Dimensional Separation, ref. 18 . . . . . | 3 |
| 2-2 | Longitudinal Pressure Distributions, 30% Bluntness, $\alpha = 10^{o}$, ref. 18 . . . . . | 3 |
| 2-3 | Circumferential Pressure Distributions, 30% Bluntness, $\alpha = 10^{o}$, ref. 18 . . . . . | 3 |
| 2-4 | Circumferential Pressure Distributions, 30% Bluntness, $\alpha = 10^{o}$, ref. 18 . . . . . | 3 |
| 2-5 | Projected Stream Surface, $M_\infty = 7.95$, $\theta = 10^{o}$, $T_w/T_o = 0.41$ ___, Sonic Line: $(u^2 + w^2)1/2/a = 1$, (a) Rex = $3.6 \times 10^5$, $\alpha = 8^{o}$, (b) Rex = $3.6 \times 10^5$, $\alpha = 10^{o}$, (c) Rex = $2.1 \times 10^5$, $\alpha = 20^{o}$, ref. 19 . . . . . | 7 |
| 2-6 | (a) Boundary-Layer Thickness, $M_\infty = 7.95$, $T_w/T_o = 0.41$, Rex = $3.6 \times 10^5$, Experimental Data (Tracy 1963); ___, Present Theory. (b) Displacement Thickness. $M_\infty = 7.95$; $\bar{x} = 1.17$ in.; Re = $1.1 \times 10^6$, $\alpha = 20^{o}$ (Above): ___ Δ; ___, $\delta_x^*$. $\alpha = 8^{o}$ (Below); ___. Δ; ___, Axisymmetric $\delta_x^*$, ref. 19. . . . . | 7 |
| 2-7 | Cross Plane Velocity Vector Distribution for Tracy's Case; $\alpha = 12^{o}$, ref. 20 . . . . . | 8 |
| 3-1 | Circular Cone with Blunted Nose . . . . . | 16 |
| 3-2 | Skin Friction Distribution on a Sharp Circular Cone. . . . . | 18 |
| 3-3 | Heat Transfer Distribution on a Sharp Circular Cone. . . . . | 18 |
| 3-4 | Longitudinal Skin Friction Distribution in Meridian Planes for a Sphere Cone . . . . . | 19 |
| 3-5 | Longitudinal Heat Transfer Distribution in Meridian Planes for a Sphere Cone . . . . . | 19 |
| 3-6 | Coordinate System for a Cone. . . . . | 21 |

ILLUSTRATIONS (CONT)


| Figure | | Page |
|---|---|---|
| 3-7a | Sphere-Cone Geometry with Location of Starting Conditions . . . . . | 22 |
| 3-7b | Coordinate System and Discretization . . . . . | 23 |
| 3-8 | Initial Velocity Profiles in $\phi$ Planes, U, Re = 1. $\times 10^6$ . . . . . | 24 |
| 3-9 | Initial Crossflow Velocity Profiles in $\phi$ Planes, W, Re = 1. $\times 10^6$ . . . . . | 25 |
| 3-10 | Initial Temperature Profiles in $\phi$ Planes, T, Re = 1. $\times 10^6$ . . . . . | 26 |
| 3-11 | Typical Inviscid Edge Conditions in the Starting Surface, Re = 1. $\times 10^6$ . . . . . | 28 |
| 4-1 | Comparison of Various Terms in 3D $x_1$ and $x_3$ Momentum Equations. Each Term Nondimensionalized by Dividing by $\rho_r U_r^2/L_r$ = 6700 lbf/ft$^3$ Laminar Flow Case . . . . . | 35 |
| 4-2 | Edge Conditions at $\tilde{x}$ = 210, $x = (x - x_o)/\delta(\phi = 0, x = x_o)$, Case I. Laminar Flow, No Cross Flow Recirculation . . . . . | 39 |
| 4-3 | Mainstream and Cross Flow Velocity Profiles Compared at Starting and Downstream Stations; Case I: Laminar Flow . . . . . | 40 |
| 4-4a | Static Pressure Variation with Distance Downstream and Azimuthal Angle for Cases I and II . . . . . | 41 |
| 4-4b | | 42 |
| B-1 | Global and Local Coordinate Systems . . . . . | 57 |

TABLES


| Number | | Page |
|---|---|---|
| 2-1 | Description of Three Cases Considered . . . . . | 10 |
| 3-1 | Sphere-Cone Geometry: Definition of Metrics for Coordinates Downstream of Sphere-Cone Junction . . . . . | 15 |
| 3-2 | Definition of Problem . . . . . | 27 |
| 4-1 | Comparison Between 2D and 3D Compressible Boundary Layers . . . . . | 34 |
| 4-2 | Mesh and Step Size Characteristics of Three Cases | 37 |
| 4-3 | $C_f/2$ Distribution Cases I and III . . . . . | 44 |
| B-1 | General Boundary Condition Statement . . . . . | 52 |
| B-2 | Implicit Definition of Simplex Natural Coordinate Functions . . . . . | 54 |
| B-3 | Integrals of Natural Coordinate Function Products Over Finite Element Domains . . . . . | 54 |
| B-4 | Standard Finite Element Matrix Forms for Simplex Functionals in One- and Two-Dimensional Space . . . . . | 55 |

## NOMENCLATURE

| | |
|---|---|
| $\bar{A}$ | Damping term in turbulence model |
| $C_{f_\xi}$ | Longitudinal skin friction coefficient defined by $C_{f_\xi} = \dfrac{\tau_{w_\xi}}{\frac{1}{2}\bar{\rho}_\infty \bar{u}_\infty^2}$ |
| $C_{f_\eta}$ | Transverse skin friction coefficient defined by $C_{f_\eta} = \dfrac{\tau_{w_\eta}}{\frac{1}{2}\bar{\rho}_\infty \bar{u}_\infty^2}$ |
| $\bar{C}_p$ | Specific heat at constant pressure |
| $d$ | Dissipation rate of turbulence |
| $\hat{e}_1, \hat{e}_2, \hat{e}_3$ | Unit vectors in curvilinear coordinate system |
| $h_1, h_2, h_3$ | Scale factors in the $x_1, x_2, x_3$-directions, respectively |
| $h_{ref}$ | Reference enthalpy defined by $h_{ref} = C_p t_{ref}$ |
| $H$ | Total enthalpy |
| $\hat{i}, \hat{j}$ | Unit vectors in Cartesian coordinate system |
| $k$ | Turbulent kinetic energy |
| $\ell$ | Mixing length |
| $\bar{L}$ | Reference length |
| $M_\infty$ | Freestream Mach number |
| Pr | Prandtl number defined to be $Pr = \dfrac{\bar{\mu}\,\bar{C}_p}{\bar{k}}$ |
| $p$ | Dimensionless pressure nondimensionalized by $p = \dfrac{\bar{p}}{\bar{\rho}_\infty \bar{u}_\infty^2}$ |
| $q$ | Dimensionless heat-transfer rate defined by $q = \dfrac{\bar{q}}{\bar{\rho}_\infty \bar{u}_\infty^3}$ |

| | |
|---|---|
| $R$ | Gas constant |
| $Re$ | Reference Reynolds number as defined by $Re = \frac{\bar{\rho}_\infty \bar{u}_\infty \bar{L}}{\bar{\mu}_{ref}}$ |
| $r$ | Distance measured from the origin of the r, $\theta$, $\phi$ coordinate system |
| $t$ | Dimensionless temperature nondimensionalized by $t = \frac{\bar{t}}{\bar{u}_\infty^2/R}$ |
| $T$ | Absolute temperature |
| $\bar{t}_{ref}$ | Reference temperature defined by $\bar{t}_{ref} = \frac{\bar{u}_\infty^2}{R}$ |
| $\bar{u}_\infty$ | Freestream velocity |
| $u,v,w$ | Velocities in $x_1,x_2,x_3$ directions |
| $x,y,z$ | Cartesian coordinates |
| $x_1,x_2,x_3$ or $\xi,\zeta,\eta$ | Curvilinear coordinates |
| $\tilde{x}$ | $= (x - x_i)/\delta(x = x_i, \phi = 0)$ |
| $x_i$ | Starting point of finite element solution region |
| $\alpha$ | Angle of attack |
| $\gamma$ | Ratio of specific heats, $\bar{C}_p/\bar{C}_v$ |
| $\bar{\gamma}$ | Intermittency function |
| $\delta$ | Boundary layer thickness |
| $\delta_{ij}$ | Kronecher delta |
| $\epsilon$ | Eddy viscosity |
| $\theta$ | Spherical coordinate system angle |
| $\mu,\lambda$ | Viscosity nondimensionalized by $\mu = \frac{\bar{\mu}}{\bar{\mu}_{ref}}$ $\bar{\mu}_{ref} = \bar{\mu}(\bar{t}_{ref})$ |

| | |
|---|---|
| $\bar{\mu}_{ref}$ | Viscosity evaluated at the reference temperature, $\bar{t}_{ref}$ |
| $\rho$ | Dimensionless density nondimensionalized by $\bar{\rho}/\bar{\rho}_\infty$ |
| $\tau_{w_\xi}$ | Longitudinal wall shear stress component |
| $\tau_{ij}, \tau$ | Viscous stress tensor |
| $\tau_{w_\eta}$ | Transverse wall shear stress component (in $\eta$-direction) |
| $\phi$ | Spherical coordinate system angle |
| $\phi_D$ | Diffusion of energy |
| $\phi_\mu$ | Dissipation of energy |
| $\omega$ | Van Driest damping factor |
| $\theta$ | Spherical coordinate system angle |

**Subscripts**

| | |
|---|---|
| e | Inviscid condition at the body surface |
| i,j,k | Indices |
| s | Static |
| t | Total |
| w | Conditions at the body surface |
| o | Stagnation conditions or at zero angle of attack |
| $\infty$ | Freestream conditions |

**Superscripts**

| | |
|---|---|
| - | Dimensional quantity |

## 1.0 SUMMARY

Numerical determination of the complete flow field description around external stores configured as blunted axisymmetric bodies at finite angle of attack is presented. The finite element computer program is employed for solution of the three-dimensional, compressible parabolic Navier-Stokes equations, which describe the complete flow field including flow separation in the cross-flow plane in the vicinity of the leeward body generator. The appropriately required initial and boundary conditions for this solution are obtained from a finite difference computer program which solves laminar compressible three-dimensional boundary layer flow around spherically blunted cones at an angle of attack. Extension of the analysis to include the turbulent transport phenomena is presented. Three numerical experiments were performed to establish the requirements of finite element network, finite element sizes, step size, and computer times. The results, which do not correspond to any specific experimental test condition or geometry, show that the numerical solution algorithm does compute the developing flow field on a blunted axisymmetric body in a convergent and stable manner.

## 2.0 INTRODUCTION

### 2.1 Background

Solution of the compressible three-dimensional boundary layer equations for flows over arbitrarily shaped external and internal configurations is a current design and analysis requirement for numerous important systems applications. It is only in the last few years that efficient numerical techniques coupled with large high speed computers have become available thereby making solution of these problems tractable, e.g., see the Proceedings of the Conference on Aerodynamic Analyses Requiring Advanced Computers, 1975[1]. Three-dimensional boundary layer solutions have been used to aid in understanding and/or designing both internal and external flow environments. For example, three-dimensional boundary layer solutions have been used to characterize mixing in scramjet combustors and chemical laser optical cavities, Zelazny et al[2, 3]. Cebeci et al[1] have developed a computer program which is optimized for wing geometries whereas Kendall et al[1] have developed a program for the external flow field about general shaped configurations for which real gas effects are important. Blottner[4] has discussed the status of the numerical computation of 3D boundary layers wherein it was noted that one of the major problems is the determination of the inviscid flow conditions. Several solutions have been reported for blunt body shapes (e.g., sphere-cone) where curve fit relations have been used to represent the pressure field with the other inviscid flow conditions being calculated, see, for example, Vvedenskaya[5] or Popinski and Davis[6].

This investigation focuses on one particular aspect of three-dimensional flows, the laminar and turbulent boundary layer developing in the leeward region for a sphere-cone body, Figure 2-1, where cross flow recirculation effects are important. This region is characterized by a strong viscous-inviscid interaction and as shown in Figure 2-1 can result in generation of separated flows. The solution is obtained using the finite element method. This method has been applied recently to problems in fluid

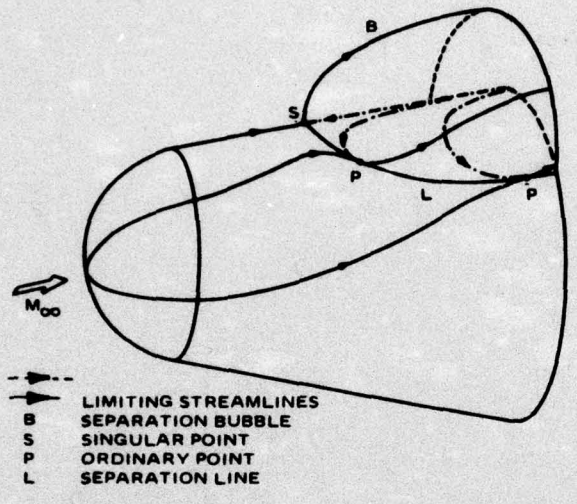


Figure 2-1. Separation Bubble Flowfield Model for Three-Dimensional Separation, ref. 18

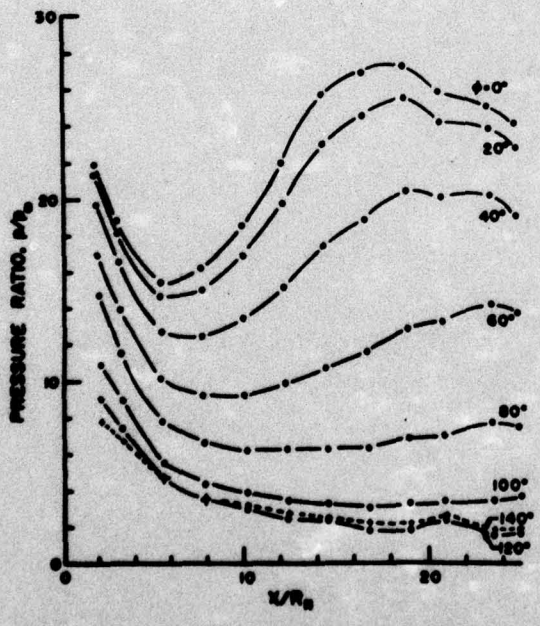


Figure 2-2. Longitudinal Pressure Distributions, 30% Bluntness, $\alpha = 10°$, ref. 18

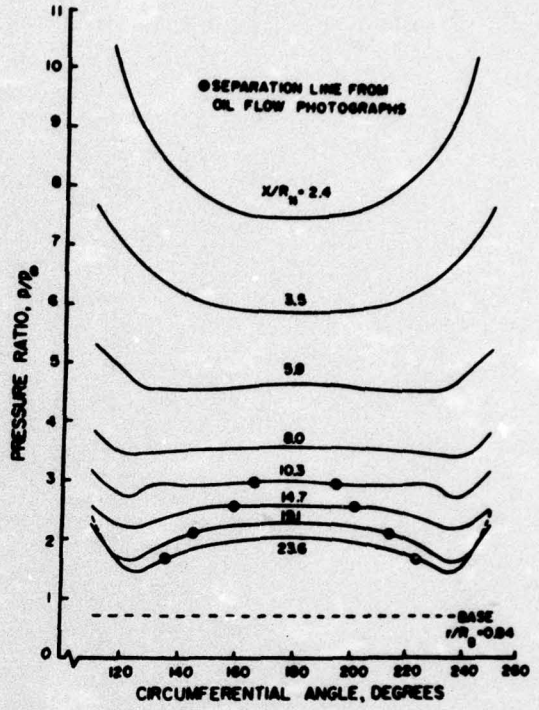


Figure 2-3. Circumferential Pressure Distributions, 30% Bluntness, $\alpha = 10°$, ref. 18

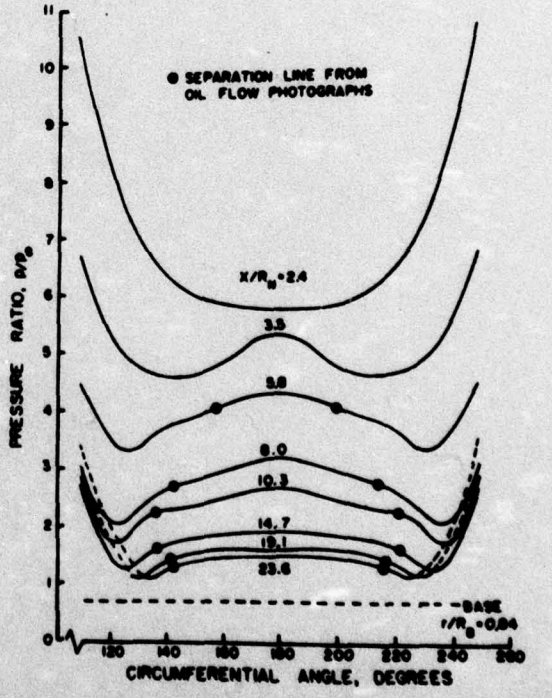


Figure 2-4. Circumferential Pressure Distributions, 30% Bluntness, $\alpha = 10°$, ref. 18

mechanics[1, 2, 3], and a comparison of the finite element and the more established finite difference method has been made recently by Popinski et al[7].

In solving the three-dimensional laminar boundary layer equations for a body at angle of attack, difficulties in obtaining solutions at the leeward symmetry plane have been encountered by many workers. Moore[8] showed that the cross-flow momentum equation has a unique asymptotic solution at certain conditions and non-uniqueness occurs otherwise. This indeterminacy was attributed by Moore to a lack of previous history in the description of the fluid entering the leeward region from the windward surface of the cone. Solutions in the leeward region have been studied by a number of investigators, e.g., Moore[9]; Cheng[10]; Vvedenskaya[5]; Libby[11, 12]; and Dwyer[13]. Murdock[14] obtained solutions in the leeward region which were not known previously, and determined conditions for which the boundary layer in this region was independent of the out-of-plane flow. He investigated cases for which the complete boundary layer solution does not exist; for this case, he concluded that the boundary layer model has a defect which results in discontinuous derivatives in the leeward plane.

Similarity three-dimensional boundary layer solutions obtained by integration around the cone in circumferential direction have been reported by a number of investigators[6, 15, 16, 17]. These boundary layer solutions give satisfactory results for most of the body surface; however, at finite angle of attack, there persist small regions centered on the leeward cone generator where no solution is possible. This region of flow around a cone at finite incidence is complex and sonic speeds in the cross-flow direction can be obtained. This in turn can yield mixed-type flow field description involving different types of equations which can lead to additional difficulty. Secondary flow separation can eventually occur in the cross-flow plane, and the presence of the reversed

flow velocities contributes to the instability of initial value computations. Additionally, the leeside boundary region is dominated by the viscous-inviscid interactions, and the assumptions of constant transverse pressure and conical outer flow may not be valid.

Thus, this leeside region enclosing the cross-flow separation exhibits distinctly non-similar behavior; in particular, lateral derivatives may be of the same order as the transverse gradients. Therefore, classical boundary layer theory fails in this region, due at least to increased boundary layer growth and strong lateral gradients. In view of the unique features of the separated flow region, the governing differential equations should include the lateral diffusion terms. In addition, non-similar external free-stream conditions (from theory or experimental flow measurements) showing distinct adverse azimuthal pressure gradients should be used. Detailed features of this type of flow have been hypothesized, and substantiated experimentally, for both sharp and blunted circular cones by Stetson[18]. Figures 2-2 to 2-4 show experimentally measured[18] surface pressure distributions in both the longitudinal and circumferential directions for the blunted cone. Adverse pressure gradients in the leeward area are well defined, and points on the locus of separating streamline are indicated.

These experimental measurements[18] indicate that the separated flow region is not in direct communication with downstream influences (base region) and that a predominant flow direction is uniformly discernible. A steady, three-dimensional equation system is derivable from the full Navier-Stokes system, under these assumptions, which contains three-dimensional convection and pressure distributions, but discards as second order the diffusion operator in the predominant flow direction (only). This parabolic equation system can be solved using downstream marching procedures associated with the classical boundary layer equations, but is a two-dimensional elliptic boundary value problem in the cross-flow plane. The most prominent additional complexity inherent with

this "parabolic Navier-Stokes" system is that the static pressure distribution has become an unknown, and methods for its solution can be used to classify various investigator's approach to their solution.

Solutions for a modified parabolic Navier-Stokes system for the sharp cone at angle of attack have been reported by Lin and Rubin[19]. In their comprehensive analysis, the equation system is solved after simplifying the transverse momentum equation by balancing the transverse pressure gradient and centrifugal forces. The required surface pressure distributions are obtained from experimental measurements. Regions of separated flow in the cross-flow plane were numerically predicted[19] in the leeside of the cone, using these pressure distributions, for angles of attack up to twice the cone half-angle. The resolution of the cross-flow separation in the leeward region is well illustrated by examining the stream surfaces in a cross-plane and the distribution of the boundary layer growth as computed by Lin and Rubin[19] and shown here in Figures 2-5 and 2-6. Lubard[20] has also performed an extensive analysis for a sharp cone, using a solution of the parabolic Navier-Stokes equations coupled with the Rankine-Hugoniot relations to jump the bowshock. For this analysis[20], the transverse momentum equation was utilized to determine surface pressure from the shock solution and good agreement was obtained with the data of Stetson[18]. Solution on the leeward side includes the separation bubble which is clearly visible in the cross-plane distribution shown in Figure 2-7 (from Ref. 20). Similar techniques using the same system of equations was used by Lubard for calculation of the flow over a blunted cone at an angle of attack. The initial conditions at the sphere-cone tangency plane were provided by a separate time dependent program[21].

## 2.2 Objectives and Approach

The objective of this study was to develop and employ a numerical analysis capability which describes the flow field on the leeward side of an external store configured as a blunted axisymmetric body at an angle of attack, e.g., Figure 2-1. In

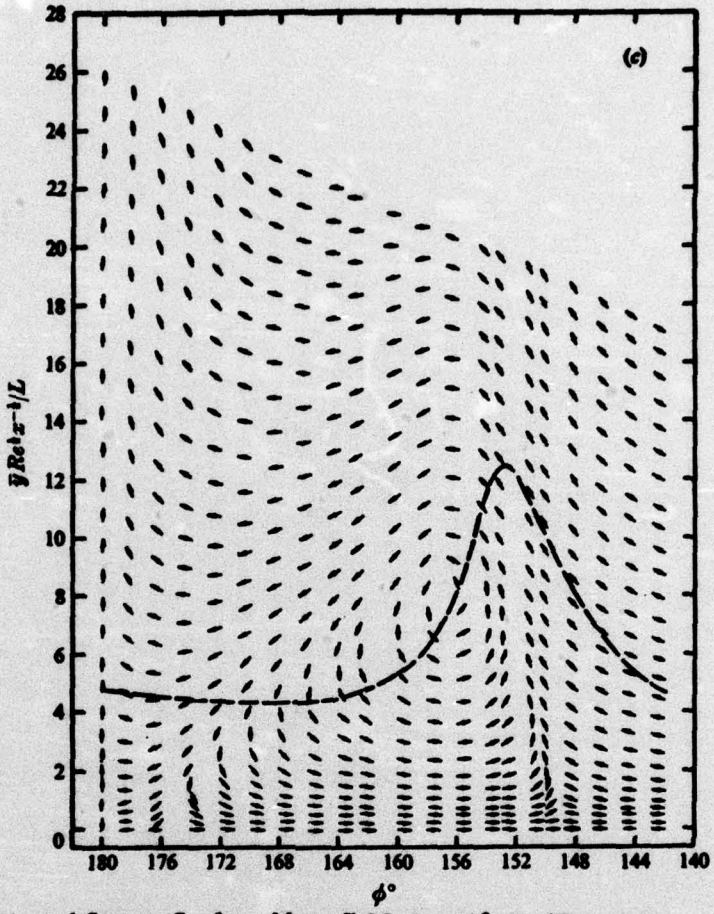


Figure 2-5. Projected Stream Surface, $M_\infty = 7.95$, $\theta = 10°$, $T_w/T_o = 0.41$ ____, Sonic Line: $(u^2 + w^2)1/2/a = 1$, (a) Rex = $3.6 \times 10^5$, $\alpha = 8°$, (b) Rex = $3.6 \times 10^5$, $\alpha = 10°$, (c) Rex = $2.1 \times 10^5$. $\alpha = 20°$, ref. 19

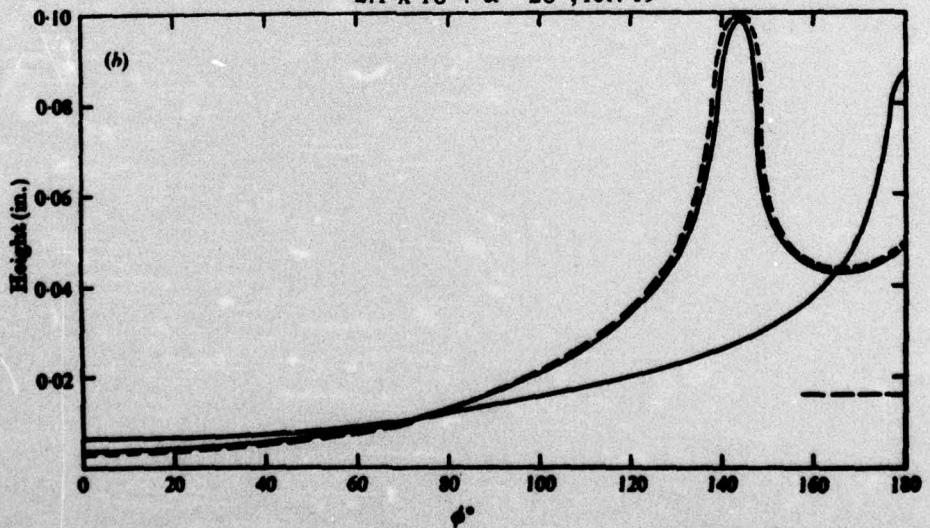


Figure 2-6. (a) Boundary-Layer Thickness, $M_\infty = 7.95$, $T_w/T_o = 0.41$, Rex = $3.6 \times 10^5$, Experimental Data (Tracy 1963); ____, Present Theory. (b) Displacement Thickness. $M_\infty = 7.95$; $\bar{x} = 1.17$ in.; Re = $1.1 \times 10^6$, $\alpha = 20°$ (Above): ____ Δ; ____, $\delta_x^*$. $\alpha = 8°$ (Below); ____. Δ; _ _ _, Axisymmetric $\delta_x^*$, ref. 19

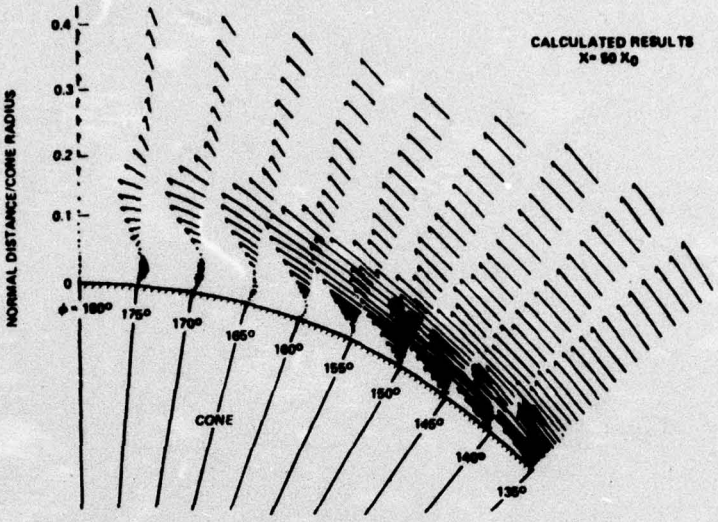


Figure 2-7. Cross Plane Velocity Vector Distribution for Tracy's Case; $\alpha = 12°$, ref. 20

addition, this analysis capability would be sufficiently general such that the boundary layers could be laminar, transitional or turbulent and cross flow recirculation effects were important and could not be neglected.

The approach taken was to merge and modify, where necessary, existing analyses (computer codes) into a viable solution technique for the external stores flow field computation. Specifically, the flow over the forward part of the blunted body was computed using an existing computer program, Popinski[22], which solves for the laminar 3D boundary layers for a sphere-cone at an angle of attack where cross flow recirculation is not important. Continuation of the solution is transferred to a second computer code for conditions where the assumption of laminar flow is invalid or cross flow diffusional effects become important. This second computer code was developed from a modification of the finite element analysis used in studies of confined (ducted) three-dimensional laminar and turbulent flows[2, 3]. This code requires a prescribed external pressure distribution which as discussed by Blottner[4] is one of the major problems with solving the three-dimensional boundary layer equations, i.e., prescribing the inviscid flow conditions. In this study, initial and inviscid conditions are used to perform numerical experiments which allow the influences of turbulence and cross flow diffusion to be isolated. Three distinct cases are considered which are defined by the combination of initial and inviscid conditions employed, Table 2-1.

The first case tests the ability of the analysis to predict the flow field on the leeward side downstream of the sphere-cone junction where cross flow diffusional effects become important. The inviscid data are based on the pressure distribution obtained using the method of characteristics, Rakich[23]. The second case examines the effect of perturbing the inviscid pressure field parametrically to induce separation in the cross flow plane. The third case examines the effect of considering transition to turbulent flow on the leeward side by "computationally" tripping

Table 2-1

Description of Three Cases* Considered

| Case | Initial Data | Inviscid Inviscid Data | Diffusion | Comments |
|---|---|---|---|---|
| I. | Generated from Finite difference program up to sphere-cone junction neglecting cross flow diffusion | Data of Rakich[23] for pressure field | Laminar | Test the ability of analysis to march into region where cross flow diffusion is important |
| II. | Same as above | Modify parametrically Rakich[23] pressure field to simulate adverse pressure gradient in cross flow direction. Examine data of Zakkay[24] to determine realistic transverse pressure distribution. | Laminar | Test the ability of the analysis to predict separation in cross flow direction |
| III. | Same as above | Same as I. | Use transitional-turbulent model at sphere-cone junction | Examine influence of trip of boundary layer to turbulent state on heat transfer characteristics |

*All cases for $10^{\circ}$ sphere-cone body at $8^{\circ}$ angle of attack.

the flow. These calculations are essential in providing the necessary familiarity of the sensitivity of theoretical predictions to critical input parameters. It is recommended that other conditions and data be examined in subsequent efforts to test the generality of the model.

The governing equations used to solve the flow field downstream of the sphere-cone junction are given in Section 3.1. The finite difference analysis used to generate the initial conditions at this junction have been reported elsewhere[6] and will not be repeated here. However, key features of the forebody flow field solution are presented in Section 3.2. Details of the inviscid pressure field and method of handling external boundary conditions are discussed in Section 3.3. Various turbulence models which have been examined and the specific approach used is described in Section 3.4. A number of well defined test cases were used in the course of this study to establish the numerical accuracy of the model and its sensitivity to discretization and step size. This effort included establishing the relative importance of the convective, diffusion, and pressure source terms in the momentum and energy equations for laminar and turbulent flows. Section 4.0 describes the results of these test cases and the results of the analysis of Cases I-III of Table 2-1. Conclusions are given in Section 5.0. Appendix A presents the results of an order of magnitude analysis which reduces the Navier Stokes equation to the parabolic form in the main flow direction. Details on the finite element solution algorithm have been reported in Refs. 2,3 and 33-37. Those modifications which were required to extend the existing program to consider the subject problem are discussed in Appendix B, Finite Element Formulation. The method used to solve the continuity equation is given in Appendix C.

## 3.0 ANALYSIS

### 3.1 Governing Equations

The governing equations in curvilinear coordinates for steady state conditions are given as follows.

Global Continuity

$$\frac{\partial}{\partial x_1}(h_2 h_3 \rho u) + \frac{\partial}{\partial x_2}(h_1 h_3 \rho v) + \frac{\partial}{\partial x_3}(h_1 h_2 \rho w) = 0 \qquad (1)$$

$x_1$ Momentum Equation

$$\frac{u}{h_1}\frac{\partial u}{\partial x_1} + \frac{v}{h_2}\frac{\partial u}{\partial x_2} + \frac{w}{h_3}\frac{\partial u}{\partial x_3} + \frac{uv}{h_1 h_2}\frac{\partial h_1}{\partial x_2} + \frac{uw}{h_1 h_3}\frac{\partial h_1}{\partial x_3}$$

$$- \frac{v^2}{h_1 h_2}\frac{\partial h_2}{\partial x_1} - \frac{w^2}{h_1 h_3}\frac{\partial h_3}{\partial x_1} = -\frac{1}{\rho h_1}\frac{\partial p}{\partial x_1} + \frac{1}{\rho}(\nabla\cdot\tau)_{x_1} \qquad (2)$$

$x_2$ Momentum Equation

$$\frac{u}{h_1}\frac{\partial v}{\partial x_1} + \frac{v}{h_2}\frac{\partial v}{\partial x_2} + \frac{w}{h_3}\frac{\partial v}{\partial x_3} + \frac{vu}{h_1 h_2}\frac{\partial h_2}{\partial x_1} + \frac{vw}{h_2 h_3}\frac{\partial h_2}{\partial x_3}$$

$$- \frac{u^2}{h_1 h_2}\frac{\partial h_1}{\partial x_2} - \frac{w^2}{h_2 h_3}\frac{\partial h_3}{\partial x_2} = -\frac{1}{\rho h_2}\frac{\partial p}{\partial x_2} + \frac{1}{\rho}(\nabla\cdot\tau)_{x_2} \qquad (3)$$

$x_3$ Momentum Equation

$$\frac{u}{h_1}\frac{\partial w}{\partial x_1} + \frac{v}{h_2}\frac{\partial w}{\partial x_2} + \frac{w}{h_3}\frac{\partial w}{\partial x_3} + \frac{wu}{h_1 h_3}\frac{\partial h_3}{\partial x_1} + \frac{wv}{h_2 h_3}\frac{\partial h_3}{\partial x_2}$$

$$- \frac{u^2}{h_1 h_3}\frac{\partial h_1}{\partial x_3} - \frac{v^2}{h_2 h_3}\frac{\partial h_2}{\partial x_3} = -\frac{1}{\rho h_3}\frac{\partial p}{\partial x_3} + \frac{1}{\rho}(\nabla\cdot\tau)_{x_3} \qquad (4)$$

Enthalpy Equation

$$\rho\left(\frac{u}{h_1}\frac{\partial H}{\partial x}+\frac{v}{h_2}\frac{\partial H}{\partial x_2}+\frac{w}{h_3}\frac{\partial H}{\partial x_3}\right) = \Phi_D + \Phi_\mu \tag{5}$$

Equation of State

$$p = \rho RT \tag{6}$$

Diffusion Coefficients

$$\mu^e = \mu + \Gamma\rho\varepsilon \tag{7a}$$

$$\mu = \mu(T) \text{ Laminar} \tag{7b}$$

$$\Gamma \equiv \text{Intermittency function} \tag{7c}$$

$$\varepsilon \equiv \text{Eddy viscosity (Section 3.5)} \tag{7d}$$

$$\frac{\mu^e}{Pr^e} = \frac{\mu}{Pr} + \frac{\rho\varepsilon}{Pr_T} \tag{7e}$$

$$Pr_T \equiv \text{Turbulent Prandtl number} \tag{7f}$$

Enthalpy-Temperature

$$T_T = T_s + \frac{u^2 + v^2 + w^2}{2C_p} \tag{8a}$$

$$C_p = C_p(T_s) \tag{8b}$$

$$H = C_p T_T \tag{8c}$$

$$T_s = T_s(H, u, v, w, C_p) \tag{8d}$$

As indicated in Section 2.0, this study was directed towards spherically blunted circular cones at an angle of attack. For this geometry, the metric coefficients $h_1$, $h_2$, $h_3$, and the required derivatives are given in Table 3-1 for a body oriented coordinate system as shown in Figure 3-1.

Examining the viscous stress tensor and performing an order of magnitude analysis (Appendix A), the governing equations result in the Equations (2), (4), and (5) simplifying to the following nondimensional form.

$$u \frac{\partial u}{\partial x_1} + v \frac{\partial u}{\partial x_2} + w \frac{\partial u}{\partial x_3} - \frac{w^2}{h_3} = - \frac{1}{\rho} \frac{\partial p}{\partial x_1} + \left[ \frac{1}{\rho} \frac{\partial}{\partial x_2} \left( \mu^e \frac{\partial u}{\partial x_2} \right) + \frac{1}{\rho h_3^2} \frac{\partial}{\partial x_3} \left( \mu^e \frac{\partial u}{\partial x_3} \right) \right] \frac{1}{Re} \tag{9}$$

$$u \frac{\partial w}{\partial x} + v \frac{\partial w}{\partial x_2} + w \frac{\partial w}{\partial x_3} + \frac{wu}{h_3} + \frac{wv}{h_3 \tan\theta_c} = \left[ - \frac{1}{\rho} \frac{1}{h_3} \frac{\partial p}{\partial x_3} + \frac{1}{\rho} \frac{\partial}{\partial x_2} \left( \mu^e \frac{\partial w}{\partial x_2} \right) + \frac{1}{\rho h_3^2} \frac{\partial}{\partial x_3} \left( \mu^e \frac{\partial w}{\partial x_3} \right) + \frac{1}{\rho h_3} \frac{\partial}{\partial x_2} \left( \mu^e \frac{\partial v}{\partial x_3} \right) \right] \frac{1}{Re} \tag{10}$$

$$\rho \left[ u \frac{\partial H}{\partial x_1} + v \frac{\partial H}{\partial x_2} + \frac{w}{h_3} \frac{\partial H}{\partial x_3} \right] = \frac{u_\infty^2}{h_{ref}} \left[ \frac{\mu}{2Re} \left( \frac{Pr-1}{Pr} \right) (u_i u_i)_{,j} \right]_{,j} + \frac{1}{Re} \left( \frac{\mu}{Pr} H_{,j} \right)_{,j} + \frac{u_\infty^2}{h_{ref} Re} \left[ (\mu u_{j,i} u_i)_{,j} + (\lambda u_{k,k} \delta_{ij} u_i)_{,j} \right] \tag{11}$$

Table 3.1

Sphere-Cone Geometry: Definition of Metrics
For Coordinates Downstream of Sphere-Cone Junction*

$$d\ell^2 = h_1^2 dx_1^2 + h_2^2 dx_2^2 + h_3^2 dx_3^2 \quad \text{(a)}$$

$$d\ell^2 = dx_1^2 + dx_2^2 + r^2 d\theta^2 \quad \text{(b)}$$

$$r \equiv x_1 \sin\phi_c + x_2 \cos\phi_c \quad \text{(c)}$$

$$r^2 d\theta^2 = (x_1 + x_2/\tan\phi_c)^2 (d\theta \sin\phi_c)^2 \quad \text{(d)}$$

$$h_1 = 1 \quad \text{(e)}$$

$$h_2 = 1 \quad \text{(f)}$$

$$h_3 = x_1 + x_2/\tan\phi_c \quad \text{(g)}$$

$$x_1 = x \quad \text{(h)}$$

$$x_2 = Y \quad \text{(i)}$$

$$x_3 = \theta \sin\phi_c \quad \text{(j)}$$

$$\frac{\partial h_3}{\partial x_1} = 1, \quad \frac{\partial h_3}{\partial x_2} = \frac{1}{\tan\theta_c} \quad \text{(k)}$$

$$\frac{\partial h_1}{\partial x_i} = \frac{\partial h_2}{\partial x_i} = 0 \quad \text{(l)}$$

*Body oriented conical coordinate system

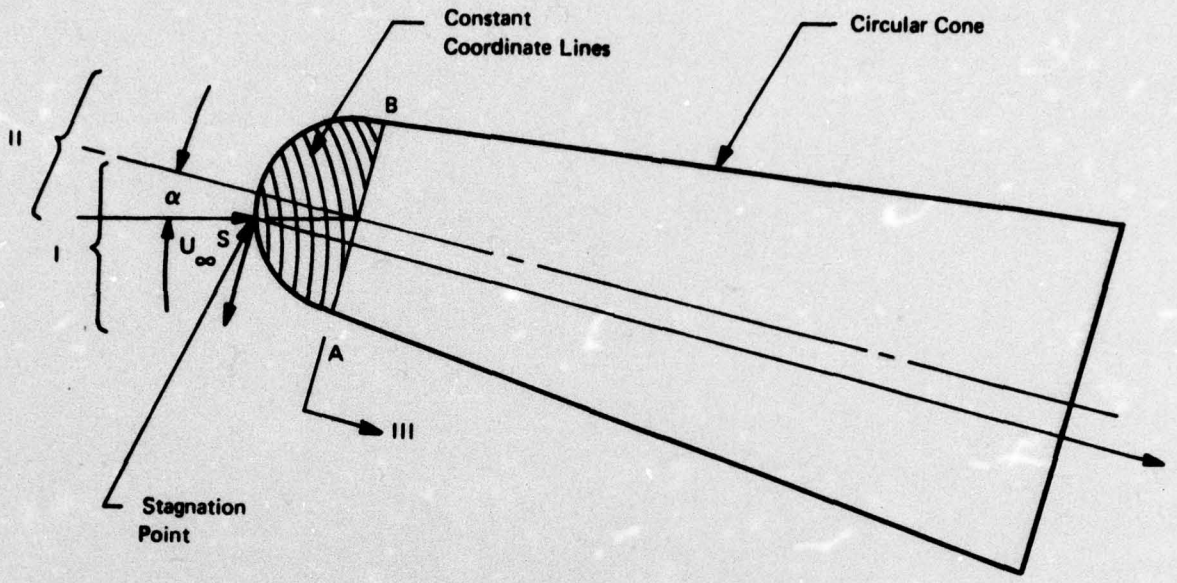


Figure 3-1. Circular Cone with Blunted Nose

In this study, the variation of pressure across the boundary layer is neglected* and Equation (2) reduces to

$$\frac{\partial p}{\partial x_2} = 0 \qquad (12)$$

The method of solution of these equations are given in Appendices B and C.

3.2 Solution of the Forebody Flow Field

In this study, an existing computer program developed by Popinski[22] was used to obtain details of the flow field in Regions I and II of Figure 3-1 and provide initial conditions along surface line AB. The stagnation point solution is determined by solving the similarity equations, obtained by a suitable transformation which eliminates dependence on the streamwise coordinate and reduces the governing equations at the stagnation point to a set of ordinary differential equations. With the known stagnation point solution, solution along the windward plane is obtained. The boundary layer solution for the stagnation region in the wind coordinate system is continued over the nose beyond the stagnation point in the body coordinate system. A change from the wind coordinate system to the body coordinate system takes place at a constant value of the surface coordinate AB (Figure 3-1). Since the constant value of the surface coordinate in the wind system does not coincide with the constant value of the surface coordinate in the body system, interpolation of the computed parameters is required.

Examples of the forebody solutions obtained using this code[6] are shown in Figures 3-2 to 3-5. Figures 3-2 and 3-3 show, for a sharp circular cone at angle of attack, computed values for skin friction and heat transfer for the classical case of constant entropy and for the case with entropy swallowing. The solution for a spherically blunted conical body at angle of attack for skin friction and heat transfer for Regions I, II, and III are shown in Figures 3-4 and 3-5. These results[6], based on solution in

*See Lubbard and Rakich[21] for an alternate approach

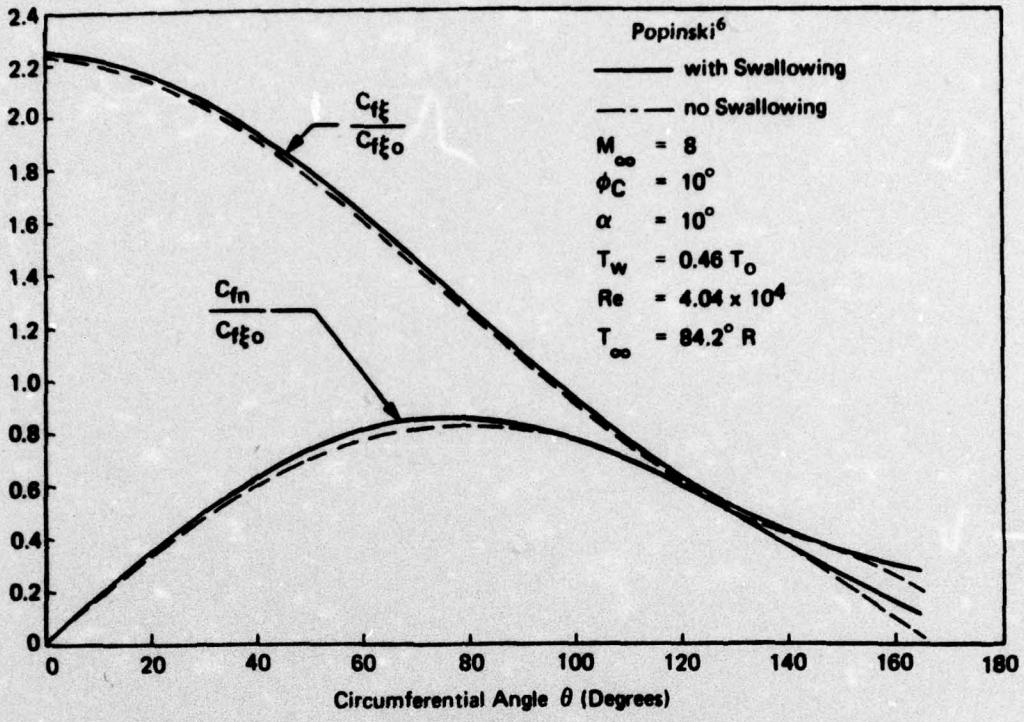


Figure 3-2. Skin Friction Distribution on a Sharp Circular Cone

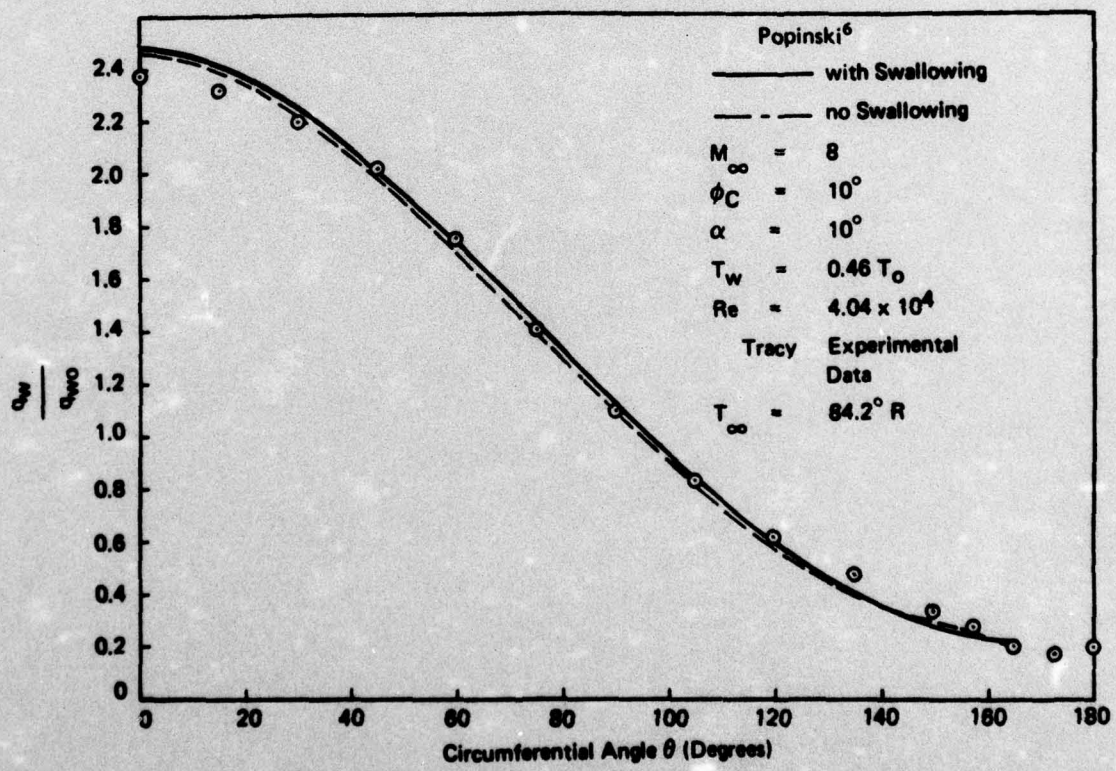


Figure 3-3. Heat Transfer Distribution on a Sharp Circular Cone

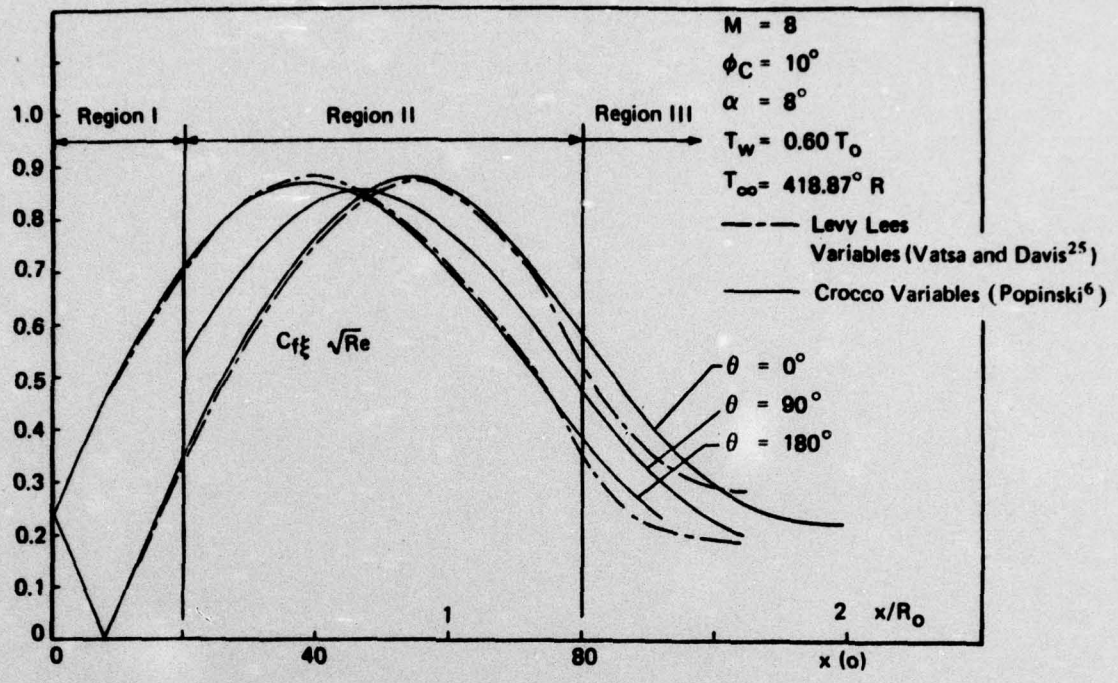


Figure 3-4. Longitudinal Skin Friction Distribution in Meridian Planes for a Sphere Cone

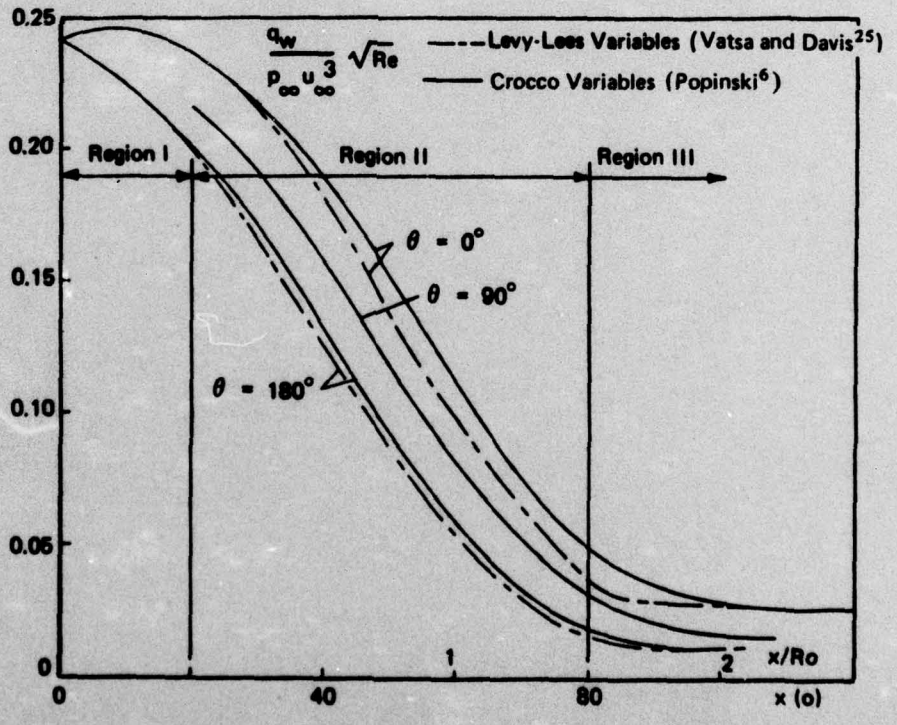


Figure 3-5. Longitudinal Heat Transfer Distribution in Meridian Planes for a Sphere Cone

Crocco variables, compare favorably with results obtained in Levy-Lees variables, Vatsa and Davis[25].

### 3.3 Initial and Boundary Conditions

The sphere-cone body under consideration as shown in Figure 3-6 identifies the coordinates $x_1$, $x_2$, $x_3$ and the corresponding velocities u, v, and w, respectively. The flow computations in this program are started downstream from the sphere-cone junction point (point CJ, Figure 3-7a). The initial values of the dependent variables needed as starting conditions were obtained using the approach described in the previous section. The computed values are stored on an external storage device (magnetic tape) and interpolation performed to obtain values at the finite element node points, e.g., Figure 3-7b. This interpolation is required since the mesh used in the finite difference forebody analysis generally must be more refined than the finite element mesh. Typical initial profiles for u, v, and T in the starting surface are shown in Figures 3-8 to 3-10 for selected meridian planes for the conditions listed in Table 3-2.

The inviscid edge conditions for the dependent variables to be used in the computations as boundary conditions have been obtained in a form compatible with the finite element step sizes. The numerical data was obtained by Rakich[23] using a three-dimensional method of characteristics. Figure 3-11 shows the circumferential distribution of the inviscid pressure p, velocities u, v, and the boundary layer thickness in the starting surface. These data are based on pressure distribution for a sphere-cone body which was generated by the method of characteristic (Rakich[23]). At this stage the circumferential pressure distribution used in the computations does not have adverse gradient in the leeward area. However, once the program is made operational, the pressure distribution will be modified accordingly to produce flow separation in the cross-flow direction in the leeward area.

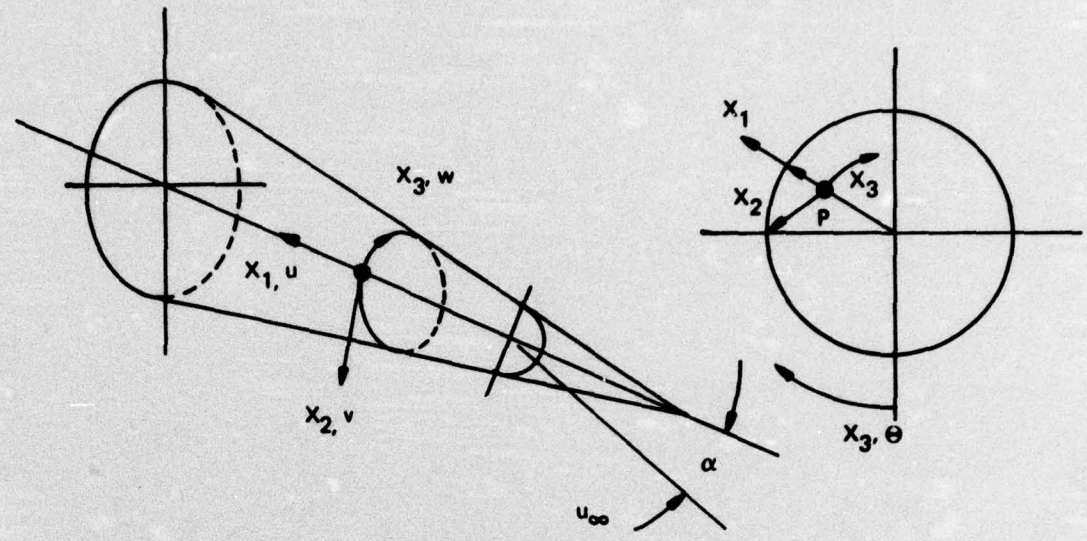


Figure 3-6. Coordinate System for a Cone

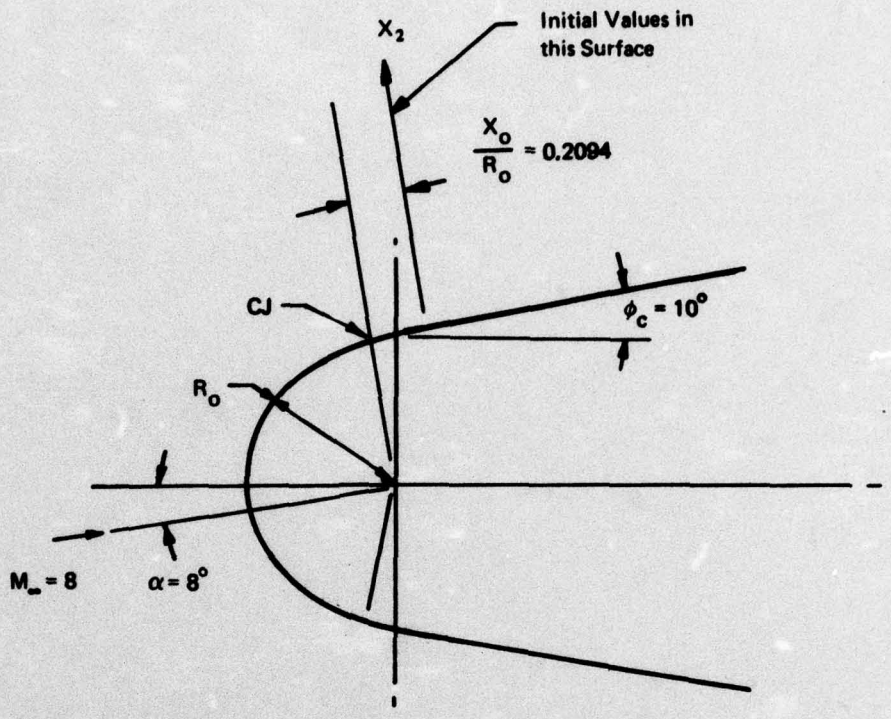


Figure 3-7a. Sphere-Cone Geometry with Location of Starting Conditions

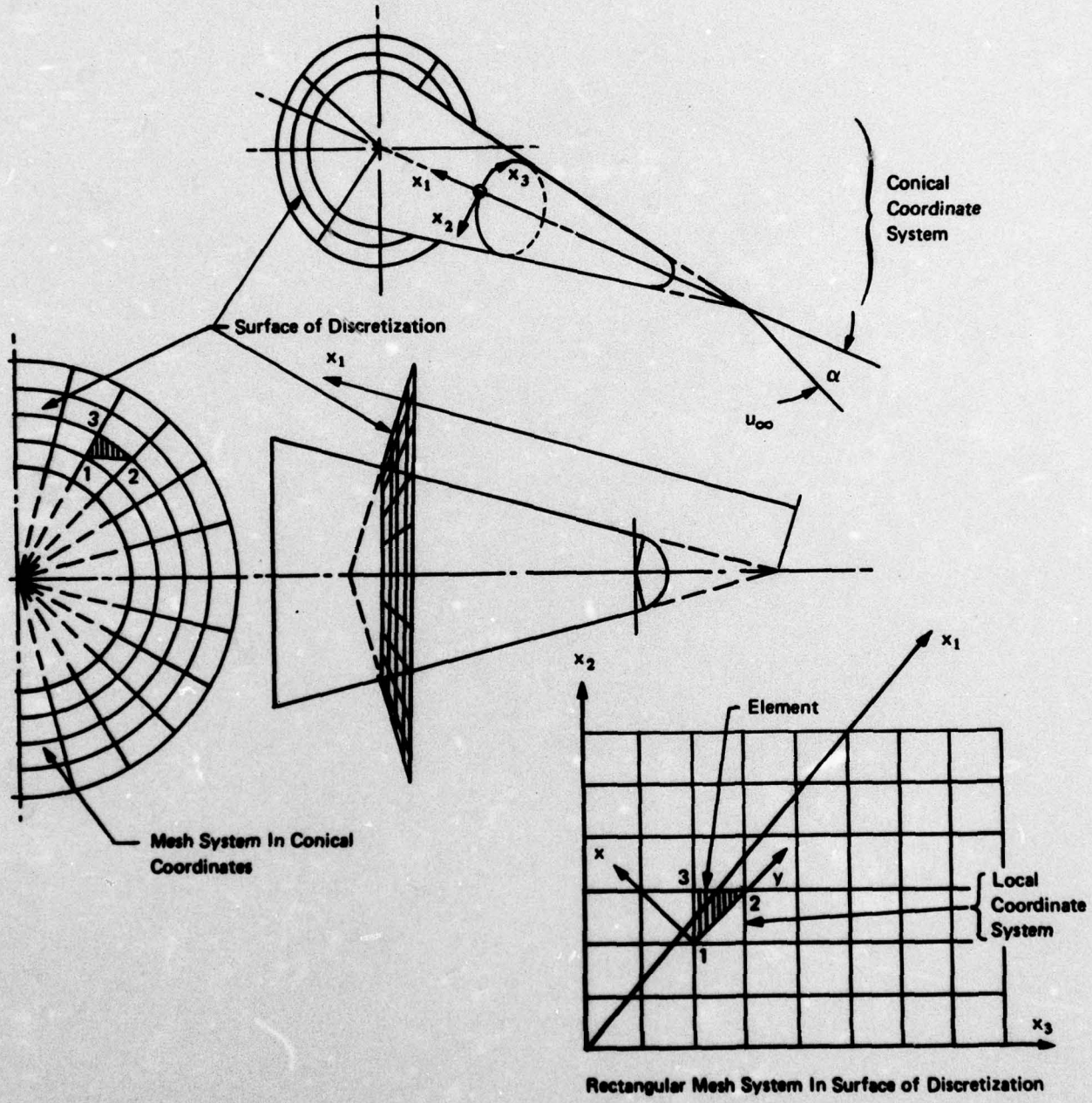


Figure 3-7b. Coordinate System and Discretization

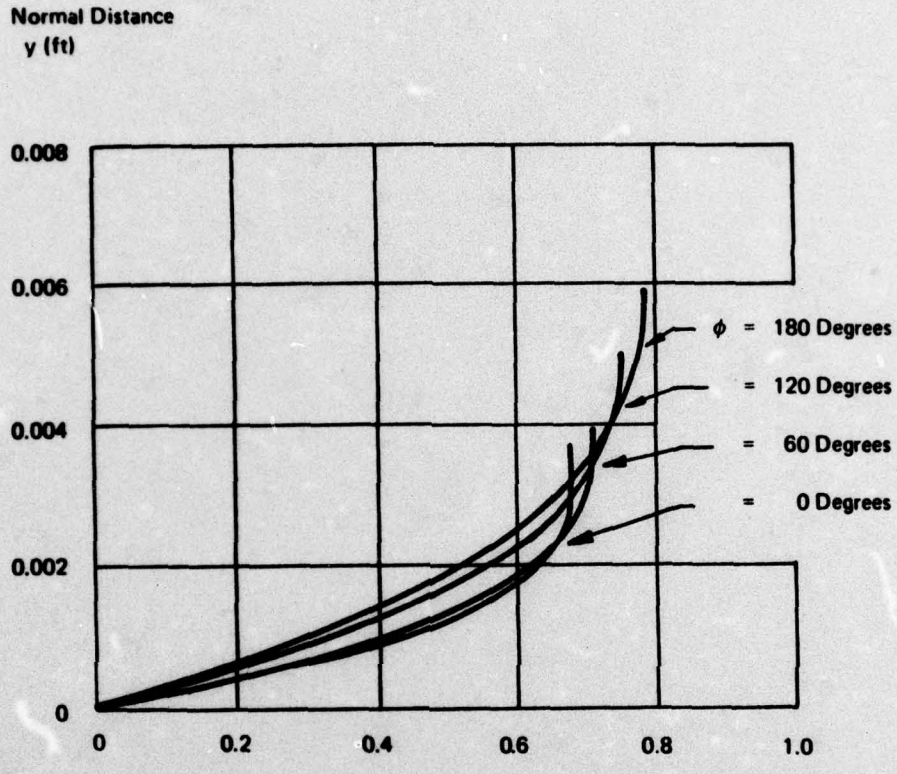


**Figure 3-8. Initial Velocity Profiles in $\phi$ Planes, U, Re = 1. x $10^6$**

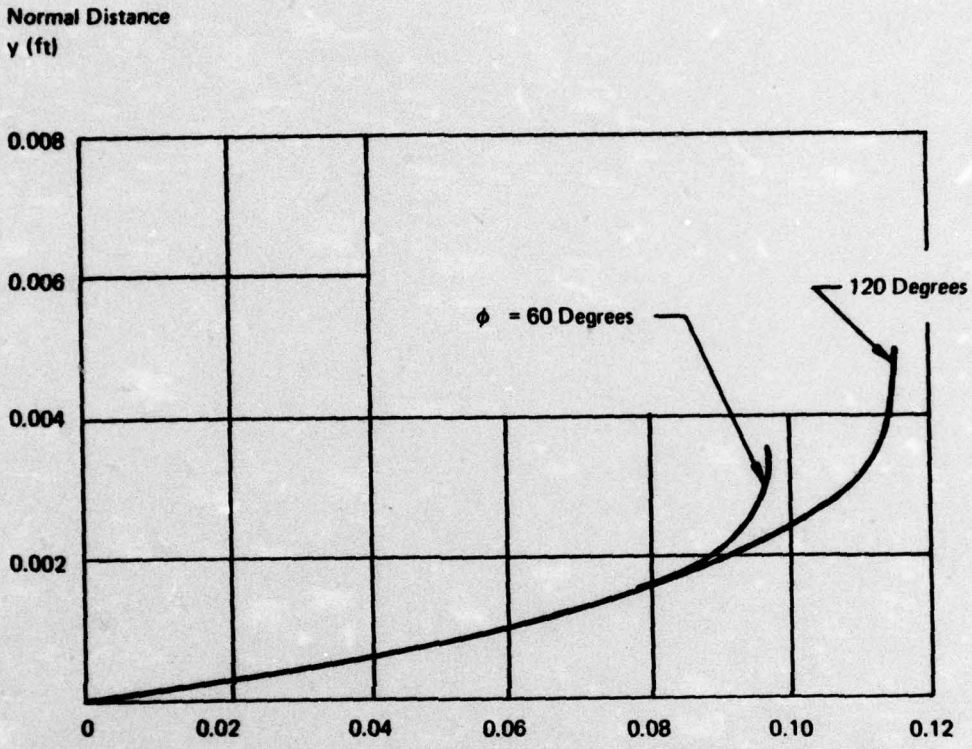


**Figure 3-9. Initial Crossflow Velocity Profiles in $\phi$ Planes, W, Re = 1. x $10^6$**

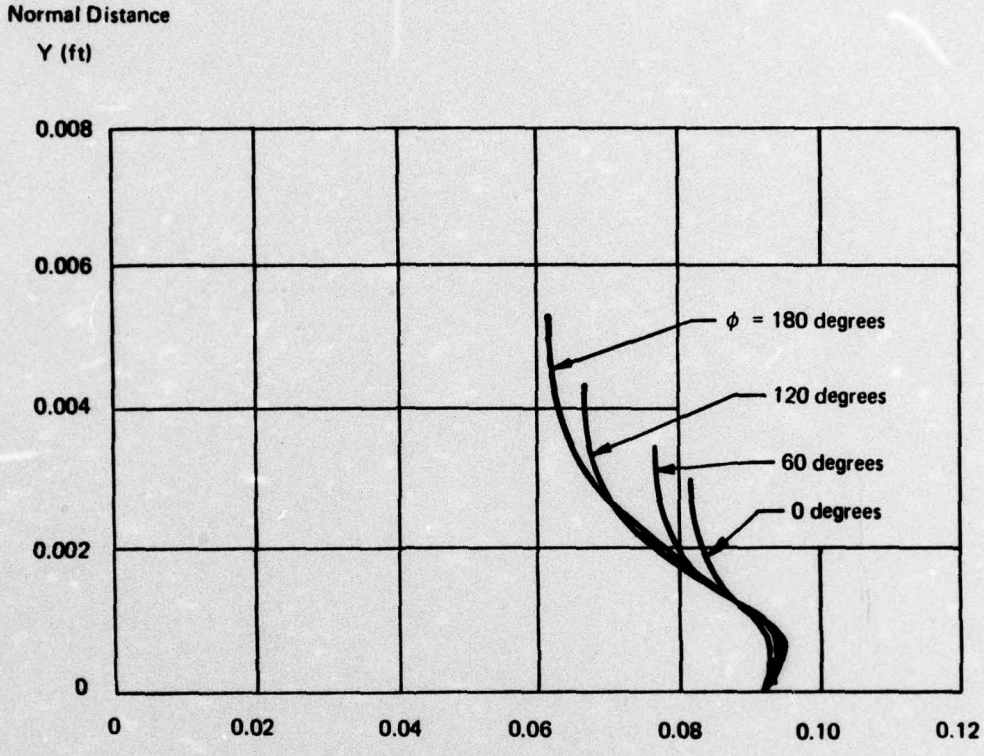


Figure 3-10. Initial Temperature Profiles in $\phi$ Planes, T, Re = 1. x $10^6$

Table 3-2

Definition of Problem

| | |
|---|---|
| Cone Half Angle, $\phi_c/2$ | $10^o$ |
| Nose Radius, $R_N$ (ft) | 1.0 |
| Angle of Attack, $\alpha$ | $8^o$ |
| Mach Number, $M_\infty$ | 8 |
| Reynolds Number, $\frac{\rho_\infty U_\infty R_N}{\mu}$ | $8\times10^5$ |
| Wall Temperature | $T_w = .6T_o$ |
| Prandtl Number, constant | 0.72 |
| Ratio of Specific Heats | 1.4 |

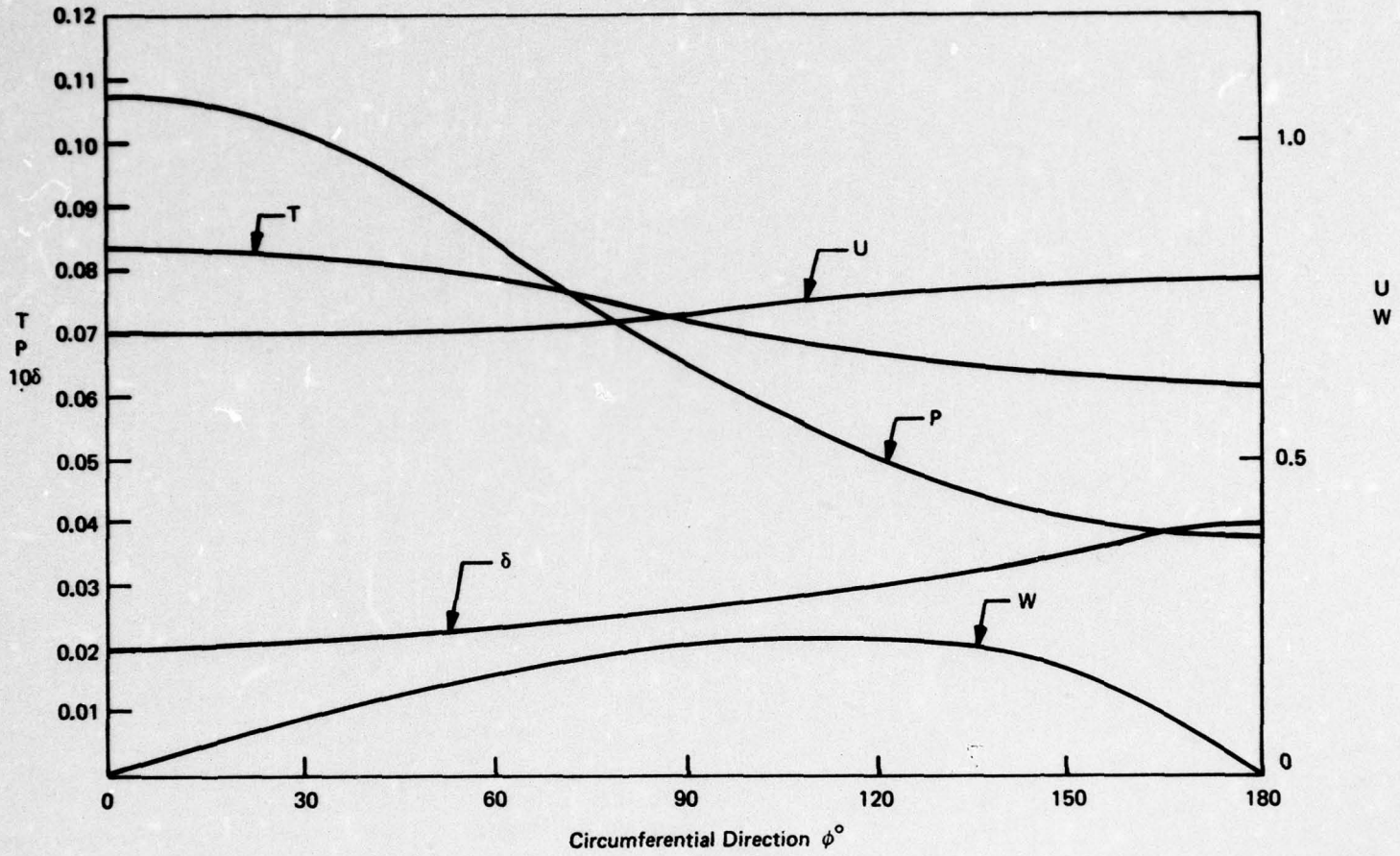


Figure 3-11. Typical Inviscid Edge Conditions in the Starting Surface, Re = 1. x $10^6$

## 3.4 Turbulence Models

### 3.4.1 Background

In laminar flows the boundary layer equations represent a closed set (equations equal dependent variables) since the viscosity, mass diffusivity, and thermal conductivity are known molecular quantities. However, when transitional, turbulent, and relaminarizing flows become important, the additional Reynolds stresses are introduced, which must be modeled empirically to complete closure of the equation system. The approaches taken in modeling the turbulent flux terms can be classified into two categories. Category I, the more common approach, involves specification of eddy coefficient models (eddy viscosity and turbulent Prandtl and Schmidt numbers). Category II can be defined as any method which introduces at least one additional equation to describe a turbulent flux or a parameter related to a turbulent flux, e.g., turbulence kinetic energy (TKE), eddy viscosity, length scale. An excellent review of the various models for turbulence is contained in Launder and Spalding[26] and more recently by Murthy[27].

It is significant that methods of Category II are becoming increasingly popular. This interest may be attributed to the success these methods have had in accurately predicting: (1) incompressible boundary layer flows (Kline et al[28]), (2) transition (Donaldson[29]), and (3) free shear layers[30]. The ability to model a wide range of flow conditions with a single set of empirical constants is the main advantage of Category II methods. This is not surprising since the physics of turbulent flow including upstream history effects is more closely modeled than methods of Category I. However, methods of Category II have certain restrictions, including: (1) requiring empirical relations to model the higher order correlations appearing in the equations (data needed to model these correlations are available only for limited flow conditions), (2) requiring initial profiles for the turbulence parameters being considered, and (3) an increase in

computer computation time due to the introduction of additional equations. It is expected that with the continuing interest and effort presently directed toward methods of Category II that these drawbacks will be overcome and that sophisticated modeling of turbulence in compressible, three-dimensional flows will be feasible soon. At this time, description of turbulence using methods of Category I appears most plausible because they have been demonstrated to yield solutions to practical problems. However, the generality of our approach will permit using methods of Category II to model turbulence as these more sophisticated techniques become proven.

The location of transition from laminar to turbulent flow is dependent on such parameters as surface roughness, freestream turbulence, Reynolds number, and pressure gradients (see Morkovin[31]). Characterization of this region is important, for in some cases it becomes larger than the laminar and turbulent regions and the peak heating often occurs within the transition zone (Masaki and Yakura[32]). At present, there is no generally successful technique for predicting transition. The transition regions have generally been specified directly as input into the solution or by using empirical correlations based upon data covering a range of flow conditions, see Harris[1].

### 3.4.2 Approach

At this time, it appears most practical to model turbulence using an eddy coefficient hypothesis. Following Harris[1], the following scalar invariant turbulence model is used

$$\varepsilon = \ell^2 \left[ \left( \frac{\partial u}{\partial x_2} \right)^2 + \frac{1}{h_3^2} \left( \frac{\partial w}{\partial x_3} \right)^2 \right]^{1/2} \tilde{\gamma} \qquad (13)$$

$$\bar{\ell} = k_2 \tanh \left( \frac{k_1}{k_2} \bar{x}_2 \right) \omega \qquad (14)$$

$$\omega = 1 - \exp\left(\frac{x_2}{\bar{A}}\right) \tag{15}$$

$$\bar{A} = k_3 \left(\frac{\mu}{\rho}\right)_w u^{*1/2} \tag{16}$$

$$\tilde{\gamma} = \frac{1 - \text{erf}(k_5 \bar{x}_2 - k_6)}{2} \tag{17}$$

Equation (7e) is used to obtain the effective Prandtl number. The constants $k_1$, $k_2$, $k_3$, $k_4$, $k_5$, $k_6$, and $N_{Pr_T}$ were assigned the values of 0.435, .09, 26., 0.01685, 5., 0.75, and 0.95, respectively.

A second turbulence model was also incorporated into the equation system which retains the concept of an eddy viscosity but relates it to the turbulence kinetic energy, k, and dissipation d as $\varepsilon = Ck^2/d$ where

$$k = \frac{q^2}{2} = (\overline{u'^2} + \overline{v'^2} + \overline{w'^2})/2 \tag{18}$$

The length scale is expressed in terms of k and the dissipation rate for turbulence, d, as

$$\ell = k^{3/2}/d \tag{19}$$

The turbulence kinetic energy equation is introduced to determine k

$$\rho \frac{Dk}{Dt} = \nabla \cdot \left(\frac{\mu_{eff}}{Pr_{k,eff}} \nabla k\right) + \tau : \nabla \vec{u} - \rho d C_D \tag{20}$$

where

$\tau$ = the effective stress tensor

$\vec{u}$ = time averaged velocity vector

$Pr_{k,eff}$ = effective Prandtl number of turbulence (empirical constant)

$C_D$ = dissipation rate constant

$\mu_{eff}$ = $\mu + \varepsilon$

In many flows with a predominant flow direction, it is often sufficient to determine the turbulent length scale by equating it with the characteristic width of the mixing region. However, in many complex flows, it is much more difficult to determine a length scale due to the complexity of the flow field. To overcome this difficulty, an additional conservation equation is introduced for the dissipation rate of turbulence

$$\rho \frac{Dd}{Dt} = \nabla \cdot \left( \frac{\mu_{eff}}{Pr_{d,eff}} \nabla d \right) + \frac{C_{d1}}{k} \tau : \nabla \vec{u} - C_{d2} \frac{d^2}{k} \qquad (21)$$

In the following section, we present the results of our efforts to modify the COMOC computer code to consider turbulence and cross flow diffusional effects and discuss future plans.

# 4.0 RESULTS

## 4.1 Check Cases

The parabolic Navier-Stokes equation system solved using the finite element solution algorithm may be routinely employed to consider two-dimensional problems over flat plates as a special case. This feature is important since changes to large computer codes easily introduce errors which often can only be detected using existing well defined solutions. In addition, the accuracy and convergence characteristics of solutions to flow fields which are less complex than the 3D flow problem of interest herein can be used to gain insight into optimum mesh size requirements, i.e., conditions which minimize computer time. With this point in mind, a compressible laminar boundary layer developing on a flat plate was successfully used to establish the accuracy of each change required to modify an existing code[2] to apply to the three-dimensional flow over blunted axisymmetric bodies.

As a second means of testing the accuracy of the modified COMOC code, the forebody solution at the sphere cone junction was analyzed in detail to determine the relative magnitude of each term in the governing equations. Table 4-1 compares the boundary layer thicknesses, velocities, pressures, temperatures, viscosities, and pressure gradients between a two-dimensional compressible boundary layer with a known analytical solution[38] and the three-dimensional boundary layer of interest in this investigation. The boundary layers on sphere cone are considerably smaller than the flat plate case due to the highly favorable pressure gradient upstream of the sphere cone junction. Figure 4-1 shows how the rate of change of momentum is distributed across the boundary layers in both the streamwise and cross flow directions at the plane which will be used to start the afterbody flow field solution. The values were obtained by using a finite

Table 4-1

Comparison Between 2D and 3D Compressible Boundary Layers

| Parameter | 2D Boundary Layer on* Flat Plate | 3D Boundary Layer at Sphere-Cone Junction** $\phi = 0^\circ$ | $\phi = 90^\circ$ | $\phi = 180^\circ$ |
|---|---|---|---|---|
| $\delta$, ft. | 0.0132 | 0.0020 | 0.0026 | 0.0039 |
| $\frac{\partial p}{\partial x}$, lbf/ft$^3$ | -19. | -20.3 | -11.0 | 0 |
| $\frac{1}{h_3}\frac{\partial p}{\partial \phi}$, lbf/ft$^3$ | 0 | 0 | -66.0 | 0 |
| $U_e$, ft/sec | 4005. | 5620. | 5862. | 6264. |
| $p_e$, lbf/ft$^2$ | 4.3 | 200. | 130. | 74. |
| $T_e$, $^\circ$K | 466. | 3230. | 2810. | 2500. |
| $\mu_e$, lbm/ft-sec | $0.112 \times 10^{-4}$ | $0.385 \times 10^{-4}$ | $0.360 \times 10^{-4}$ | $0.336 \times 10^{-4}$ |
| $\nu_e$, ft$^2$/sec | 0.0637 | 0.031 | 0.039 | 0.0569 |
| $U_e\delta/\nu_e$ | 830. | 363. | 391. | 429. |

*Similarity solution from Ref. 38 for $M_e = 5$, $\beta = 0.5$, $U_e\delta/\nu_e = 830$.

**Forebody solution for conditions listed in Table 3-2 .

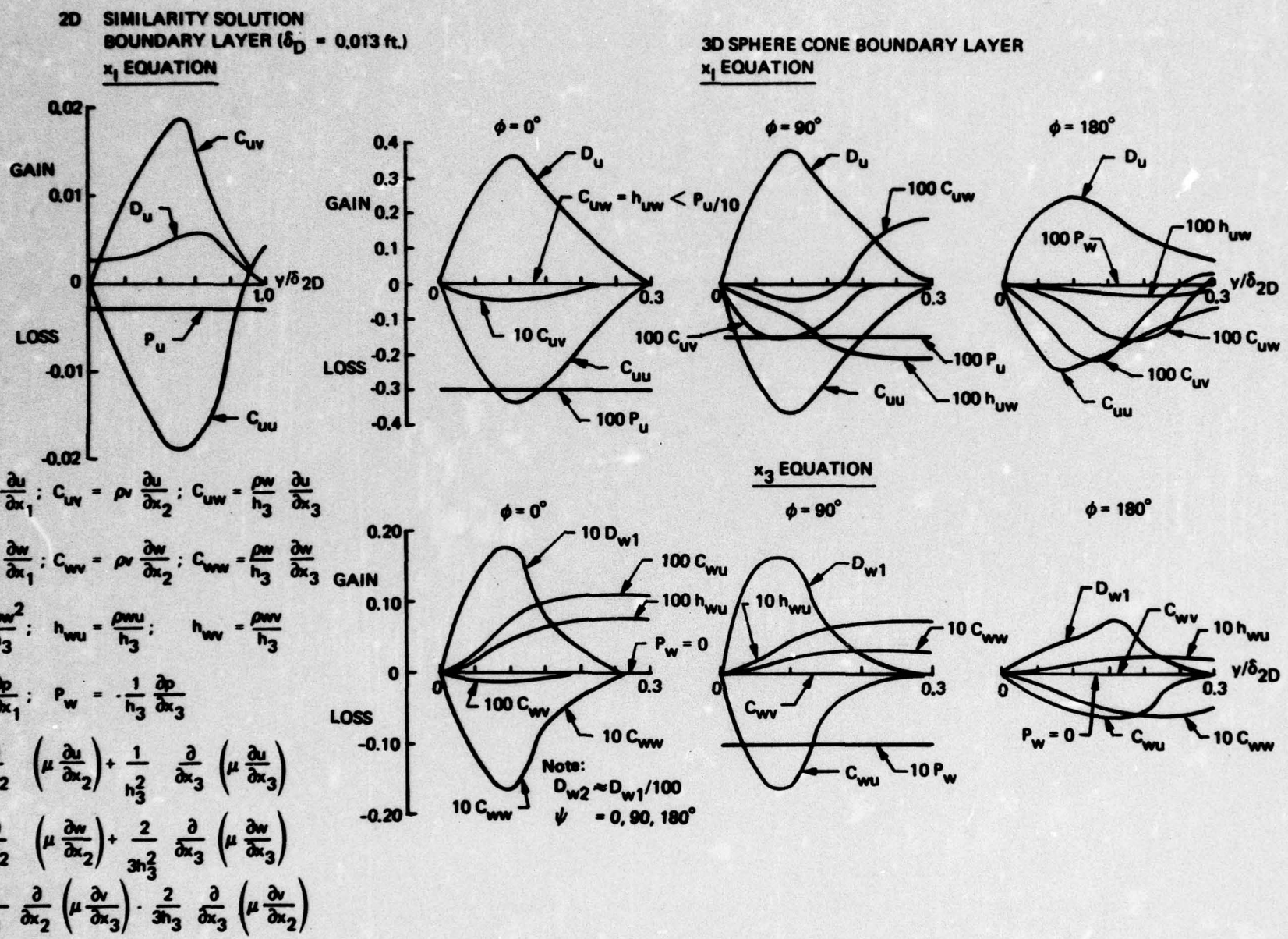


$$C_{uu} = \rho u \frac{\partial u}{\partial x_1}; \quad C_{uv} = \rho v \frac{\partial u}{\partial x_2}; \quad C_{uw} = \frac{\rho w}{h_3} \frac{\partial u}{\partial x_3}$$

$$C_{wu} = \rho u \frac{\partial w}{\partial x_1}; \quad C_{wv} = \rho v \frac{\partial w}{\partial x_2}; \quad C_{ww} = \frac{\rho w}{h_3} \frac{\partial w}{\partial x_3}$$

$$h_{uw} = -\frac{\rho w^2}{h_3}; \quad h_{wu} = \frac{\rho w u}{h_3}; \quad h_{wv} = \frac{\rho w v}{h_3}$$

$$P_u = -\frac{\partial p}{\partial x_1}; \quad P_w = -\frac{1}{h_3} \frac{\partial p}{\partial x_3}$$

$$D_u = \frac{\partial}{\partial x_2} \left( \mu \frac{\partial u}{\partial x_2} \right) + \frac{1}{h_3^2} \frac{\partial}{\partial x_3} \left( \mu \frac{\partial u}{\partial x_3} \right)$$

$$D_{w1} = \frac{\partial}{\partial x_2} \left( \mu \frac{\partial w}{\partial x_2} \right) + \frac{2}{3h_3^2} \frac{\partial}{\partial x_3} \left( \mu \frac{\partial w}{\partial x_3} \right)$$

$$D_{w2} = \frac{1}{h_3} \frac{\partial}{\partial x_2} \left( \mu \frac{\partial v}{\partial x_3} \right) - \frac{2}{3h_3} \frac{\partial}{\partial x_3} \left( \mu \frac{\partial v}{\partial x_2} \right)$$

Figure 4-1. Comparison of Various Terms in 3D $x_1$ and $x_3$ Momentum Equations. Each Term Nondimensionalized by Dividing by $\rho_T U_T^2 / L_T$ = 6700 lbf/ft$^3$ Laminar Flow Case

difference technique to compute each term for comparison with the corresponding terms in the finite element code. These results were then used to aid in program checkout and gain insight into the dominant mechanisms governing the boundary layer development. The two-dimensional boundary layer is also shown for comparison. The primary difference between the character of the 2D and 3D flows is that for the sphere-cone body the boundary layer is being accelerated at a much higher rate (more than a factor of 10) in both the $x_1$ and $x_3$ directions. The larger accelerations associated with the three-dimensional boundary layers result in a stiffer system of differential equations than the corresponding 2D problem and consequently longer computer solution times are required as shown below.

## 4.2 Demonstration Cases

Table 2-1 showed three cases used in this study to examine the performance of the finite element numerical solution algorithm in characterizing three-dimensional boundary layer flows. Items of particular interest were computer solution time requirements, the number of finite elements needed to assure convergence and required step size. The initial values for the flow region being considered are taken downstream of the sphere-cone junction point as shown in Figure 3-7a. The mesh size, number of steps, distance marched downstream and computer time requirements are given in Table 4-2 for all three cases. Calculations made with additional nodes show no significant effect (< 4% differences of $\tilde{x} = 330$) on computed values downstream. Using less nodes in either the y or $\phi$ direction resulted in unstable solutions. The length coordinate, $\tilde{x}$, was selected to reflect the number of initial boundary layer thicknesses (at $\phi = 0$) which have been marched downstream of the starting location. Hence, $\tilde{x} = 333$ corresponds to a distance of $x = 6.88$ ft since $\delta(x = x_i, \phi = 0^o) = .003$ ft and $x_i = 5.88$ ft.

Table 4-2. Mesh and Step Size Characteristics of Three Cases

| | Case I: Laminar Flow, $\frac{\partial p}{\partial z} < 0$, $\phi > 0$ | Case II: Laminar Flow, $\frac{\partial p}{\partial z} \leq 0$, $\phi \leq 135^{o}$ | Case III: Turbulent Flow $\frac{\partial p}{\partial z} < 0$, $\phi > 0$ |
|---|---|---|---|
| Number of Nodes | 270 (10×27) | 270 (10×27) | 270 (10×27) |
| Extent of Calculation, $\tilde{x}$ (max) | 330 | | 170 |
| No. of Steps to $\tilde{x}$ (max) | 166 | | 183 |
| IBM 360/65 Time Required, hr | 1.96 | 1.96 | 1.96 |

The edge values of pressure velocities, temperature, and boundary layer thickness at $\tilde{x} = 330$ are shown in Figure 4-2 for Case I. No significant differences over the values at $\tilde{x} = 0$ are observed (see Figure 3-11) although the boundary layer thickness has increased approximately a factor of twenty over the initial values. The ten node points used across the boundary layer were found sufficient provided transverse length scale (y) was normalized by the boundary layer thickness. Computational experiments were made to determine that over 65 nodes would be required to provide the same degree of accuracy had the solution been obtained in physical coordinates. The velocity (U and W) profiles computed for Case I are shown in Figure 4-3.

The second case considered represented a perturbation about Case I where the only parameter changed was the external pressure distribution as shown in Figure 4-4a. The pressure variation at $\tilde{x} = 330$ was found to induce a cross flow recirculation pattern at $\tilde{x} = 115$ as shown in Figure 4-4b. This result clearly demonstrates the ability of the finite element solution algorithm to predict a smooth and stable development of the recirculation pattern induced by the adverse pressure distribution prescribed on the leeward side of the sphere cone body.

The third case studied considered the effect of replacing the laminar flow viscosity model with an effective viscosity composed of the sum of the laminar and turbulent viscosities, Equation (20). Three types of turbulence models were considered: (1) mixing length theory, (2) turbulence kinetic energy, Equation (20), and (3) the two-equation turbulence model, Equations (20) and (21). The finite element solution algorithm was modified to consider each of the turbulence models, however, computer time limitations* allowed for only the turbulent mixing length

*Note that computer times for solutions from $\tilde{x} = 0$ to $\tilde{x} = 170$ with Equation (20) were estimated to be 2.6 hours, whereas using both Equations (20) and (21) result in computer times of approximately 3.3 hours (IBM 360/65).

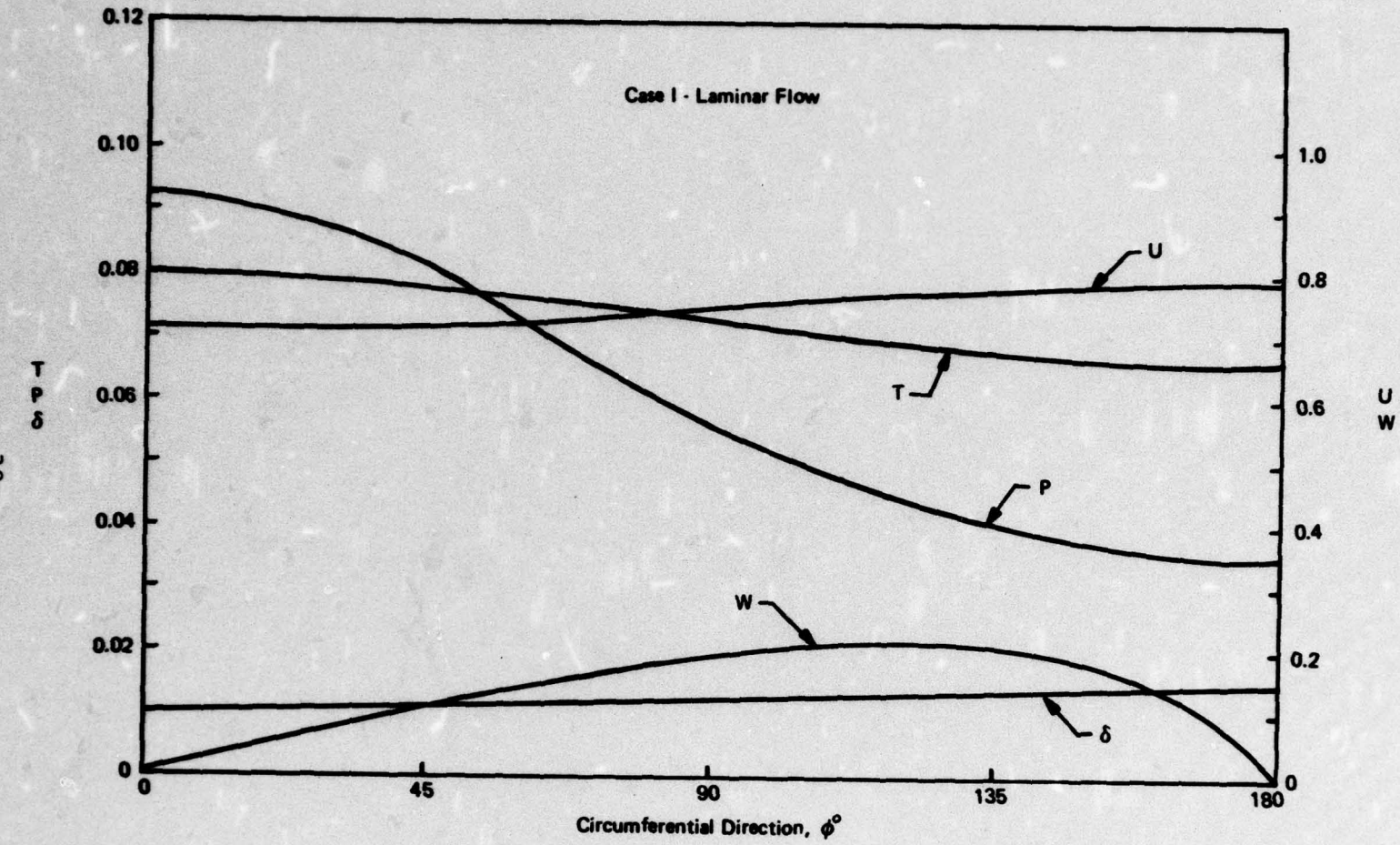


Figure 4-2. Edge Conditions at $\tilde{x} = 330$, $\tilde{x} = (x - x_o) / \delta (\phi = 0, x = x_o)$, Case I. Laminar Flow, No Cross Flow Recirculation

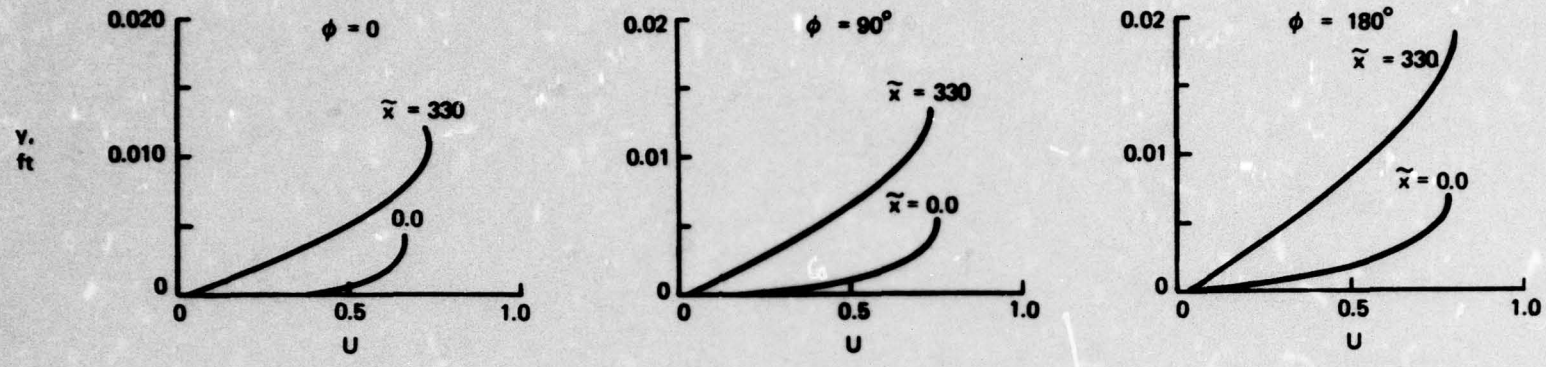


(a) Main Stream Profiles, U(y)

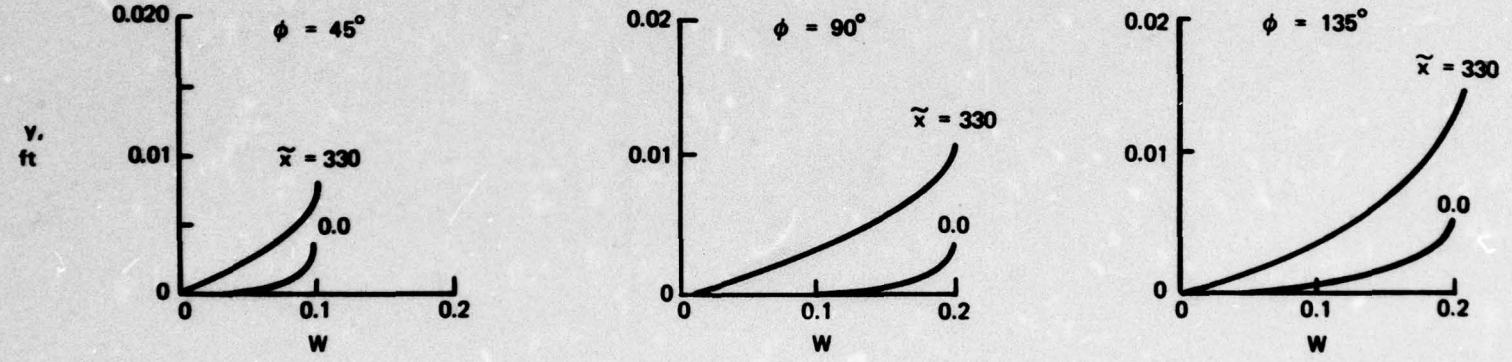


(b) Cross Flow Profiles, W(y)

Figure 4-3. Main Stream and Cross Flow Velocity Profiles Compared at Starting and Down Stream Stations; Case I: Laminar Flow

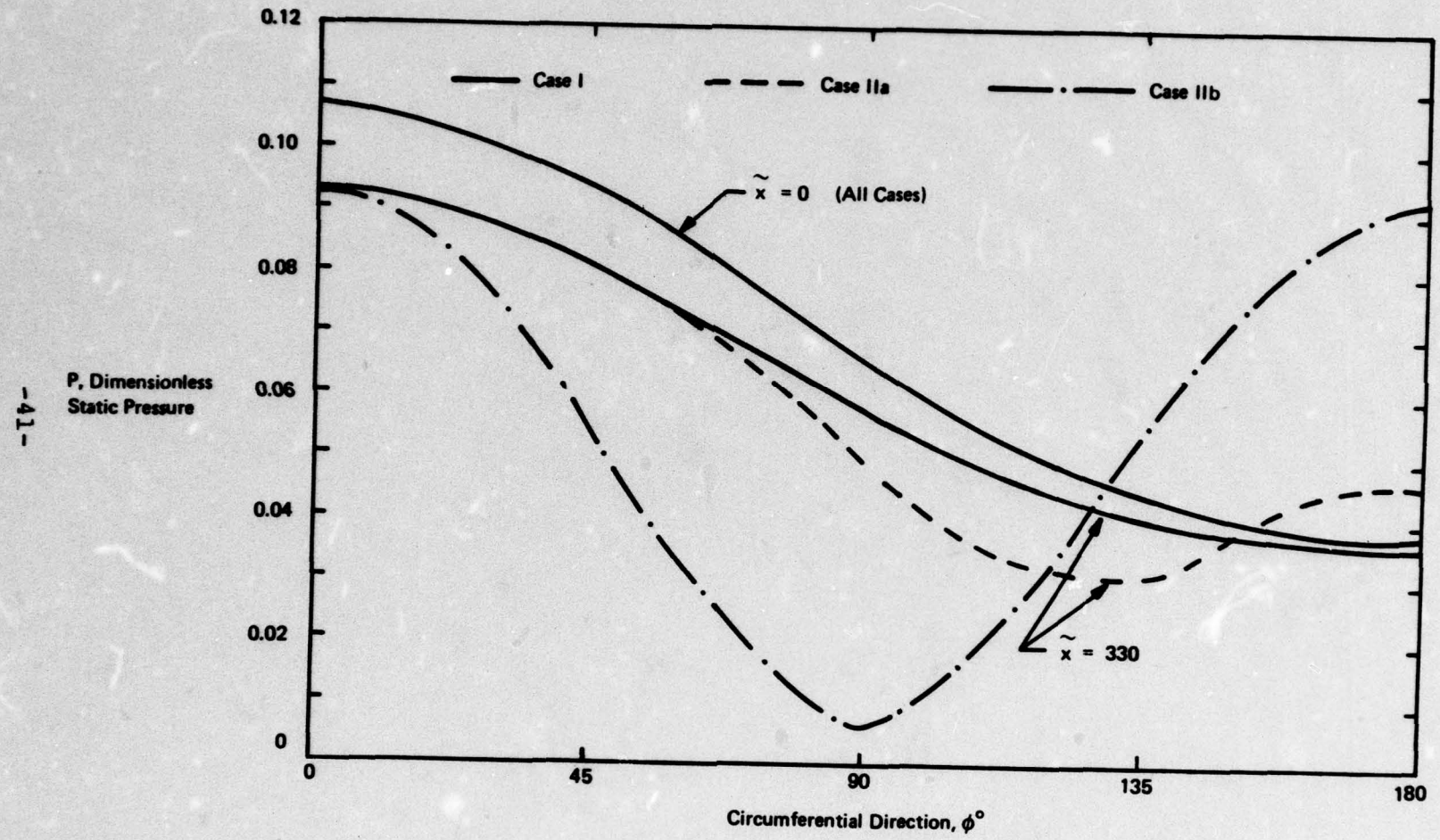


Figure 4-4a. Static Pressure Variation with Distance Downstream and Azimuthal Angle for Cases I and II

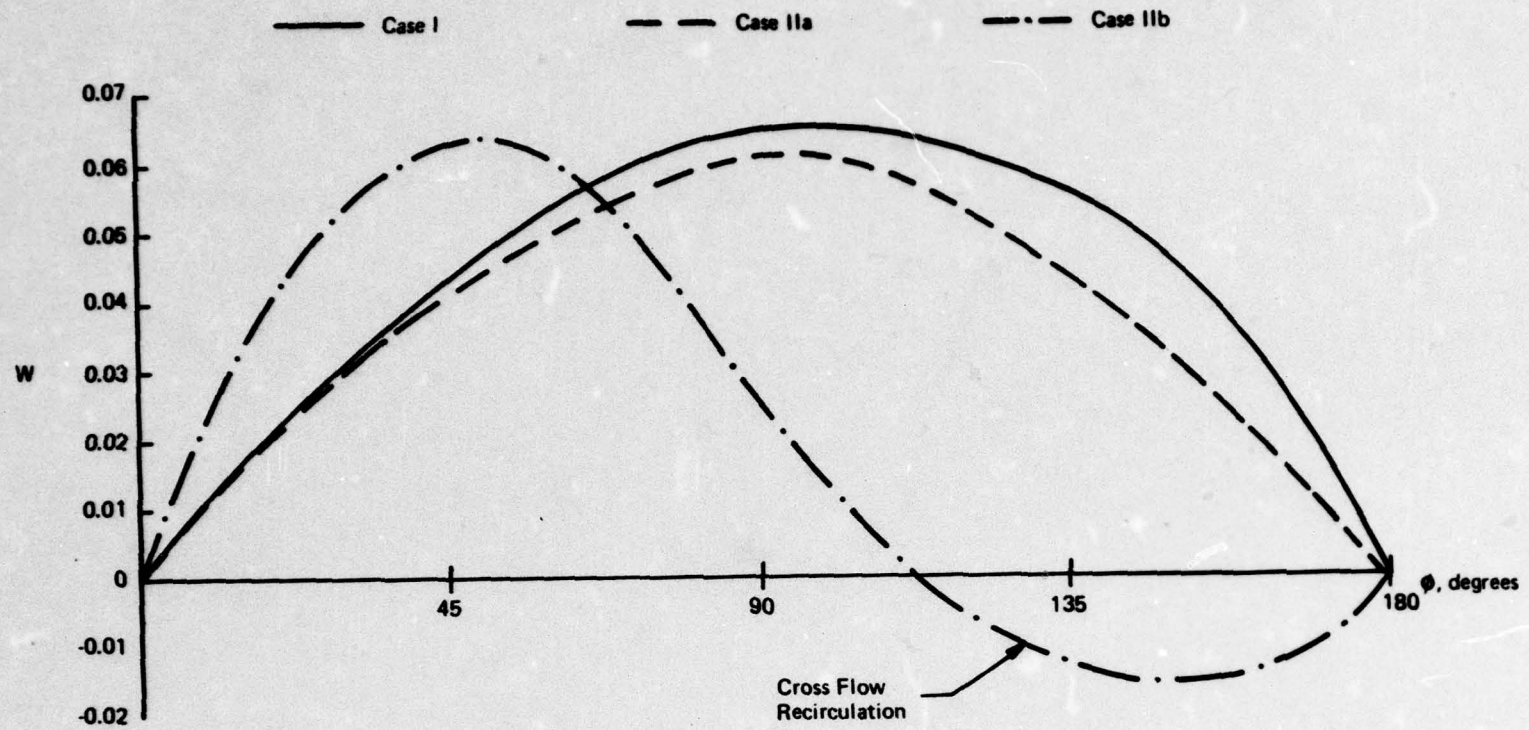


Figure 4-4b. Predicted Cross Flow Velocity Profiles at $\tilde{x}$ = 115 at $y/\delta = 0.10$ for Pressure Profiles shown in Figure 4-4a

model to be exercised over a distance downstream sufficiently large to make comparisons with Case I. The cost of the turbulent flow computation is almost twice that of the laminar calculation due to the faster mixing rate and consequently increased rate of change of the dependent variables. Table 4- compares the predicted skin friction distribution at $\tilde{x} \leq 170$ for $\phi = 0$, 90, and $180^{o}$. As expected, the "numerical tripping" of the flow at $\tilde{x} = 0$ results in an increase in the skin friction by as much as 100% over the laminar value at $\tilde{x} = 170$.

Table 4-3. $C_f/2$ Distribution* Cases I and III

| | Laminar (Case I) | | | Turbulent (Case III) | | |
|---|---|---|---|---|---|---|
| | $\phi$ (degrees) | | | $\phi$ (degrees) | | |
| $\tilde{x}$ | 0 | 90 | 180 | 0 | 90 | 180 |
| 0 | .350 | .476 | .465 | .350 | .476 | .465 |
| 17 | .219 | .248 | .233 | .245 | .279 | .260 |
| 40 | .168 | .180 | .172 | .234 | .252 | .236 |
| 93 | .134 | .136 | .116 | .226 | .235 | .191 |
| 173 | .115 | .111 | .094 | .211 | .229 | .191 |

*All values are multiplied by $\times 10^2$

## 5.0 CONCLUSIONS

The finite element solution algorithm used in the COMOC code has been extended to consider cross flow recirculation effects on blunted axisymmetric bodies at a finite angle of attack. This recirculation is induced by an externally applied "surface" pressure distribution which produced separation on the leeward side of the body. Three numerical experiments were performed to establish the requirements of finite element network, finite element sizes, step size, and computer times. The results, which do not correspond to any specific experimental test condition or geometry, show that the numerical solution algorithm does compute the developing flow field on a blunted axisymmetric body in a convergent and stable manner.

## 6.0 REFERENCES


1. Proceedings of the Conference on Aerodynamic Analyses Requiring Advanced Computers, Parts I and II, NASA SP-347, March 1975.

2. Zelazny, S. W., Baker, A. J. and Rushmore, W. L, "Modeling of Three-Dimensional Mixing and Reacting Ducted Flows," NASA CR-2661, April 1976 (see also AIAA 76-49, January 1976, for abbreviated version).

3. Zelazny, S. W. and Rushmore, W. L., "Three-Dimensional Mixing Effects in Laser Optical Cavities," presented at the AFWL Tri-Service Chemical Laser Symposium, February 1976.

4. Blottner, F. G., "Computational Techniques for Boundary Layers," AGARD LS-73, February 1975.

5. Vvedenskaya, N. D., "Calculation of the Boundary Layer Arising in a Flow About a Cone under an Angle of Attack," Zh. vychisl. Mat. mat. Fizl, Vol. 6, 1966, pp. 304-312.

6. Popinski, Z. and Davis, R. T., "Three-Dimensional Compressible Laminar Boundary Layers on Sharp and Blunted Cones at Angle of Attack," NASA CR-112316, January 1973.

7. Popinski, Z. and Baker, A. J., "An Implicit Finite Element Algorithm for the Boundary Layer Equations," Journal of Computational Physics, May 1976.

8. Moore, F. K., "Laminar Boundary Layer on Cone in Supersonic Flow at Large Angle of Attack," NACA Rep. 1132, 1953.

9. Moore, F. K., "Laminar Boundary Layer on Cone in Supersonic Flow at Large Angle of Attack," NACA TN 2844, 1952.

10. Cheng, H. K., "The Shock Layer Concept and Three-Dimensional Hypersonic Boundary Layers," Cornell Aeronautical Laboratory Report No. AF-1285-A-3, 1961.

11. Libby, P. A., "Heat and Mass Transfer at a General Three-Dimensional Stagnation Point," AIAA Journal, Vol. 5, 1967, pp. 507-517.

12. Libby, P. A. and Liu, T. M., "Some Similar Laminar Flows Obtained by Quasi-Linearization," AIAA Journal, Vol. 6, 1968, pp. 1541-1548.

13. Dwyer, H. A., "Boundary Layer on a Hypersonic Sharp Cone at Small Angle of Attack," AIAA Journal, Vol. 9, 1971, pp. 277-284.

14. Murdoch, J. W., "The Solutions of Sharp Cone Boundary Layer Equations in the Plane-of-Symmetry," The Aerospace Corporation Report MOTR-0172(S2816-60)-1, San Bernardino Operations, July 15, 1971.

15. Cooke, J. C. and Hall, M. G., "Boundary-Layers in Three-Dimensions," Progress in Aeronautical Sciences: Boundary-Layer Problems, Edited by D. Kuchemann and A. Ferri, Vol. II, Pergamon Press, New York, 1962.

16. McGowan, J. J. and Davis, R. T., "Development of a Numerical Method to Solve the Three-Dimensional Compressible Laminar Boundary-Layer Equations with Application to Elliptical Cones at Angle of Attack," Report ARL-70-0341, December 1970.

17. Boericke, R. R., "The Laminar Boundary Layer on a Cone at Incidence in Supersonic Flow," AIAA Paper No. 70-48, 1970.

18. Stetson, K. F., "Boundary-Layer Separation on Slender Cones at Angle of Attack," AIAA Journal, May 1972, pp. 642-648.

19. Lin, T. C. and Rubin, S. G., "Viscous Flow Over a Cone at Moderate Incidence-I, Hypersonic Tip Region," Computers and Fluids, Vol. 1, 1973, pp. 37-57, and "Viscous Flow Over a Cone at Moderate Incidence, Part 2, Supersonic Boundary Layer," Journal of Fluid Mechanics, Vol. 59, Part 3, 1973, pp. 593-620.

20. Lubard, S. C. and Helliwell, W. S., "Calculation of the Flow on a Cone at High Angle of Attack," AIAA Paper No. 73-636, July 1973.

21. Lubard, S. C. and Rakich, J. V., "Calculation of the Flow on a Blunted Cone at a High Angle of Attack," AIAA Paper 75-149, January 1975.

22. Popinski, Z., "Three-Dimensional and Compressible Laminar Boundary Layers on Sharp and Blunt Circular Cones at Angle of Attack," PhD Dissertation, University of Cincinnati, Department of Aerospace Engineering, 1973.

23. Rakich, J. V., "A Method of Characteristics for Steady Three-Dimensional Supersonic Flow with Application to Inclined Bodies of Revolution," NASA TND-5341, October 1969.

24. Zakkay, V., Economos, C. and Alzner, E., "Leeside Flow Field Description Over Cones at Large Incidence," AFFDL-TR-74-19, July 1974.

25. Vatsa, V. R. and Davis, R. T., "The Use of Levy-Lees Variables in Three-Dimensional Boundary-Layer Flows," University of Cincinnati, Department of Aerospace Engineering, NASA CR-112315, January 1973.

26. Launder, B. E. and Spalding, D. B., Mathematical Models of Turbulence, Academic Press, 1972.

27. Murthy, S. N. B., Turbulent Mixing in Non Reactive and Reactive Flows, Plenum Press, New York and London, 1975.

28. Kline, S. J., Morkovin, M. V., Sovran, G. and Cockrell, D. J., Editors, Proceedings, Computation of Turbulent Boundary Layers, Stanford University, 1968.

29. Donaldson, C. duP., "A Computer Study of an Analytical Model of Boundary Layer Transition," AIAA Journal, Vol. 7, 1969, pp. 271-278.

30. Free Turbulent Shear Flows, Vol. I - Conference Proceedings, NASA-Langley Research Center, NASA SP-321, July 20-21, 1972.

31. Morkovin, M. V., "Critical Evaluation of Transition from Laminar to Turbulent Shear Layers with Emphasis on Hypersonically Traveling Bodies," AFFDL-TR-68-149, March 1969.

32. Masaki, M. and Yakura, J. K., "Transitional Boundary Layer Consideration for the Heating Analysis of Lifting Reentry," Journal of Spacecraft and Rockets, Vol. 6, No. 9, September 1969, pp. 1048-1053.

33. Baker, A. J. and Zelazny, S. W., "A Theoretical Study of Mixing Downstream of Transverse Injection into a Supersonic Boundary Layer," NASA CR-112254, 1972.

34. Baker, A. J., "Finite Element Solution Algorithm for Viscous Incompressible Fluid Dynamics," International Journal of Numerical Methods in Engineering, Vol. 6, No. 1, 1973, pp. 89-101.

35. Baker, A. J., "Numerical Solution to the Dynamics of Viscous Fluid Flow by a Finite Element Algorithm: A First Step Towards Computational Continuum Mechanics," Proceedings International Association for Shell Structures Pacific Symposium on Hydromechanically Loaded Shells, 1971.

36. Zelazny, S. W. and Baker, A. J., "Predictions in Environmental Hydrodynamics Using the Finite Element Method, II. Applications," AIAA Journal, Vol. 12, No. 12, December 1974, pp. 43-46.

37. Baker, A. J., "Finite Element Computational Theory for Three-Dimensional Boundary Layer Flow," AIAA Paper 72-108, 1972.

38. Christian, J. W., Hankey, W. L., and Petty, J. S., "Similar Solutions of the Attached and Separated Compressible Laminar Boundary Layer with Heat Transfer and Pressure Gradient," Aerospace Research Laboratories Report No. ARL 70-0023, February 1970.

## Appendix A

## Order of Magnitude Analysis

The solution to the blunted cone flow at angle of attack is based on an approximate system of equations which is obtained from the steady Navier-Stokes equations. These equations are derived by introducing the assumptions that the streamwise derivatives are small as compared with the normal and circumferential derivatives $\frac{\partial}{\partial x_1} << \frac{\partial}{\partial x_2}, \frac{\partial}{\partial x_3}$ and that all velocities are of the order $\sigma(1)$. Terms of the order $\sigma(1)$ and $\sigma(\delta)$ are retained in all equations.

The divergence of the viscous shear stress tensor for laminar flow is given in curvilinear coordinates by Equations A-1 to A-3 before dropping lower order terms.

$(\nabla \cdot \tau)_{x_1}$ =

$$\frac{1}{h_1 h_2 h_3}\left[\frac{\partial}{\partial x_1}(h_2 h_3 \tau_{11}) + \frac{\partial}{\partial x_2}(h_1 h_3 \tau_{12}) + \frac{\partial}{\partial x_3}(h_1 h_2 \tau_{31})\right]$$

$$+ \tau_{12}\frac{1}{h_1 h_2}\frac{\partial h_1}{\partial x_2} + \tau_{31}\frac{1}{h_1 h_3}\frac{\partial h_1}{\partial x_3}$$

$$- \tau_{22}\frac{1}{h_1 h_2}\frac{\partial h_2}{\partial x_1} - \tau_{33}\frac{1}{h_1 h_3}\frac{\partial h_3}{\partial x_1} \qquad \text{A-1}$$

$(\nabla \cdot \tau)_{x_2}$ =

$$\frac{1}{h_1 h_2 h_3}\left[\frac{\partial}{\partial x_1}(h_2 h_3 \tau_{12}) + \frac{\partial}{\partial x_2}(h_1 h_3 \tau_{22}) + \frac{\partial}{\partial x_3}(h_1 h_3 \tau_{23})\right]$$

$$+ \tau_{12}\frac{1}{h_1 h_2}\frac{\partial h_2}{\partial x_1} + \tau_{23}\frac{1}{h_2 h_3}\frac{\partial h_2}{\partial x_3}$$

$$- \tau_{11}\frac{1}{h_1 h_2}\frac{\partial h_1}{\partial x_2} - \tau_{33}\frac{1}{h_2 h_3}\frac{\partial h_3}{\partial x_2} \qquad \text{A-2}$$

$$(\nabla\cdot\tau)_{x_3} =$$

$$\frac{1}{h_1h_2h_3}\left[\frac{\partial}{\partial x_1}(h_2h_3\tau_{31}) + \frac{\partial}{\partial x_2}(h_1h_3\tau_{23}) + \frac{\partial}{\partial x_3}(h_1h_2\tau_{33})\right]$$

$$+ \tau_{31}\frac{1}{h_1h_3}\frac{\partial h_3}{\partial x_1} + \tau_{23}\frac{1}{h_2h_3}\frac{\partial h_3}{\partial x_2}$$

$$- \tau_{11}\frac{1}{h_1h_3}\frac{\partial h_1}{\partial x_3} - \tau_{22}\frac{1}{h_2h_3}\frac{\partial h_2}{\partial x_3} \qquad \text{A-3}$$

As a result of the order of magnitude analysis, the following expressions for the viscous stress tensor terms were obtained and used in the parabolic Navier-Stokes equations.

$$\lambda\nabla\cdot\bar{V} = \lambda\left(\frac{v}{h_2h_3}\frac{1}{\tan\theta_c} + \frac{1}{h_2}\frac{\partial v}{\partial x_2} + \frac{1}{h_3}\frac{\partial w}{\partial x_3}\right) \qquad \text{A-4}$$

$$\tau_{11} = \lambda\nabla\cdot\bar{V} \qquad \text{A5-a}$$

$$\tau_{22} = \lambda\nabla\cdot\bar{V} + 2\mu\frac{1}{h_2}\frac{\partial v}{\partial x_2} \qquad \text{A5-b}$$

$$\tau_{33} = \lambda\nabla\cdot\bar{V} + 2\mu\left(\frac{1}{h_3}\frac{\partial w}{\partial x_3} + \frac{v}{h_2h_3}\frac{1}{\tan\theta_c}\right) \qquad \text{A5-c}$$

$$\tau_{12} = \frac{\mu}{h_2}\frac{\partial u}{\partial x_2} \qquad \text{A5-d}$$

$$\tau_{13} = \frac{\mu}{h_3}\frac{\partial u}{\partial x_3} \qquad \text{A5-e}$$

$$\tau_{23} = \mu\left(\frac{1}{h_2}\frac{\partial w}{\partial x_2} + \frac{1}{h_3}\frac{\partial v}{\partial x_3}\right) \qquad \text{A5-f}$$

## Appendix B

## Finite Element Formulation and Solution

The solution of the viscous flow within the cross-flow separation region as formulated by the derived parabolic Navier-Stokes system is obtained using an extension of an existing finite element computer program. The finite element code has been applied within the last few years to a family of elliptic and parabolic initial boundary value problems in fluid mechanics (Refs. 2, 3, 33-37), and their relative merits as compared with the finite difference methods have been recently evaluated[7]. The COMOC code is based on a finite element numerical solution algorithm for general systems of nonlinear elliptic boundary value partial differential equations that are also initial-value, i.e., parabolic. The general differential equation, written on a generalized dependent variable q within domain R, for which the finite element algorithm is established, is of the form,

$$(\rho uq)_{,1} = (kq_{,i})_{,i} - (\rho u_i q)_{,i} + f(qq_{,i}) \qquad \text{B-1}$$

subject to constraints on the closure $\partial R$, identified with unit normal vector $n_i$, of the form $B(q) \equiv 0$, or explicitly:

$$B(q) = a^{(1)}q + a^{(2)}kq_{,i}n_i - a^{(3)} = 0 \qquad \text{B-2}$$

For the subject problem class, the generalized diffusion term will contain the viscosity coefficients, $\mu$ and $\lambda$, and the $a^{(i)}$ are user-specified constraints enforcing all forms of physically acceptable boundary conditions, Table B-1. Solution of Equations 9-11 is accomplished by using the finite element solution algorithm. Briefly (Refs. 33 to 36), approximate the dependent variable, q, within M disjoint interior subdomains $R_m$ of R, defined by $(x_2, x_3, x_1) \varepsilon R_m \times [x_1^0, \infty)$, where the union of $R_m$ is R, by a series expansion of the form:

## TABLE B-1
## GENERAL BOUNDARY CONDITION STATEMENT

| Boundary Conditions | $a^{(1)}$ | $a^{(2)}$ | $a^{(3)}$ |
|---|---|---|---|
| No Slip at Wall | 1 | 0 | 0 |
| Slip at Wall | + | -1 | 0 |
| Mass Injection | 0 | 1 | + |
| Adiabatic Wall | 0 | 1 | 0 |
| Specified Heat Flux | 0 | 1 | + |
| Temperature Dependent Flux | + | 1 | + |
| Symmetry Condition | 0 | 1 | 0 |

+User specified as non-zero to enforce desired condition level.

$$q_m^*(x_i) \equiv \{L(x_2,x_3)\}^T\{Q(x_1)\}_m \qquad \text{B-3}$$

In Equation B-3, the elements of the column matrix $\{Q\}_m$ are the (unknown) values of q at the nodes of $R_m$, and the elements of $\{L\}$ are known polynomials (Equation B-7).

The natural coordinates $\{L\}$ of any point in the discretization plane are expressed implicitly in terms of the coordinates of the nodes in the local coordinate system (Table B-2). The finite element solution algorithm applicable to elliptic partial differential equations which is of the form:

$$\int_{R_m} W\phi^*_{,kk}\,d\tau = \int_{R_m} Wf_1(\phi^*,\phi^*_{,k},x_1)\,d\tau + \oint_{\partial R_m} Wf_2(\phi^*)\,d\sigma \qquad \text{B-4}$$

where $\phi^*$ is the approximation to the dependent variable, $f_i$ are specified functions of their arguments and contain no second derivatives of $\phi^*$, and the weighting functions W are identical to the approximation function for $\phi^*$. Within a finite element

$$\phi_m^* \equiv \{L\}^T\{\phi\}_m \qquad \text{B-5}$$

$$W \equiv \{L\} \qquad \text{B-6}$$

and in two-dimensional plane of discretization

$$\{L\} = \begin{Bmatrix} 1 - \frac{x}{x_2} + (\frac{x_3}{x_2} - 1)\frac{y}{y_a} \\ \frac{x}{x_2} - \frac{x_3}{x_2}\frac{y}{y_3} \\ \frac{y}{y_3} \end{Bmatrix} \qquad \text{B-7}$$

and

## TABLE B-2
## IMPLICIT DEFINITION OF SIMPLEX NATURAL COORDINATE FUNCTIONS

| Dimensions | Element | Nodes | Natural Coordinate Definition |
|---|---|---|---|
| 1 | Line | 2 | $\begin{bmatrix} 1 & 1 \\ x_1 & x_2 \end{bmatrix} \begin{Bmatrix} L_1 \\ L_2 \end{Bmatrix} = \begin{Bmatrix} 1 \\ x \end{Bmatrix}$ |
| 2 | Triangle | 3 | $\begin{bmatrix} 1 & 1 & 1 \\ x_1 & x_2 & x_3 \\ y_1 & y_2 & y_3 \end{bmatrix} \begin{Bmatrix} L_1 \\ L_2 \\ L_3 \end{Bmatrix} = \begin{Bmatrix} 1 \\ x \\ y \end{Bmatrix}$ |
| 3 | Tetrahedron | 4 | $\begin{bmatrix} 1 & 1 & 1 & 1 \\ x_1 & x_2 & x_3 & x_4 \\ y_1 & y_2 & y_3 & y_4 \\ z_1 & z_2 & z_3 & z_4 \end{bmatrix} \begin{Bmatrix} L_1 \\ L_2 \\ L_3 \\ L_4 \end{Bmatrix} = \begin{Bmatrix} 1 \\ x \\ y \\ z \end{Bmatrix}$ |

## TABLE B-3
## INTEGRALS OF NATURAL COORDINATE FUNCTION PRODUCTS OVER FINITE ELEMENT DOMAINS

| Dimensions | Integrals* |
|---|---|
| 1 | $\int_R L_1^{n_1} L_2^{n_2} \, dx = D \frac{n_1! \, n_2!}{(1+n_1+n_2)!}$ |
| 2 | $\int_R L_1^{n_1} L_2^{n_2} L_3^{n_3} \, dxdy = D \frac{n_1! \, n_2! \, n_3!}{(2+n_1+n_2+n_3)!}$ |
| 3 | $\int_R L_1^{n_1} L_2^{n_2} L_3^{n_3} L_4^{n_4} \, dxdydz = D \frac{n_1! \, n_2! \, n_3! \, n_4!}{(3+n_1+n_2+n_3+n_4)!}$ |

* D = Determinant of coefficient matrix defining the natural coordinate system, see Table B-2.

## TABLE B-4

## STANDARD FINITE ELEMENT MATRIX FORMS FOR SIMPLEX FUNCTIONALS IN ONE- AND TWO-DIMENSIONAL SPACE

| Matrix[1] Name | Matrix Function | Matrix Evaluation[2],[3],[4] |
|---|---|---|
| {B10} | $\int_{R_m} \{\phi\} d\tau$ | $\frac{A^m}{3}\begin{Bmatrix}1\\1\\1\end{Bmatrix}$ |
| [B211S] | $\{\phi\}_{,k}\{\phi\}^T_{,k}$ | $\left(\frac{1}{X2P2}\right)^2\begin{bmatrix}1 & -1 & 0\\ & 1 & 0\\ & & 0\end{bmatrix}$ $+\left(\frac{1}{X3P3}\right)^2\begin{bmatrix}\left(\frac{X3P3}{X2P2}-1\right)^2 & \frac{X3P3}{X2P2}\left(\frac{X3P3}{X2P2}-1\right) & \left(\frac{X3P3}{X2P2}-1\right)\\ & \left(\frac{X3P3}{X2P2}\right)^2 & -\left(\frac{X3P3}{X2P2}\right)\\ & & 1\end{bmatrix}$ |
| [B200S] | $\int_{R_m} \{\phi\}\{\phi\}^T d\tau$ | $\frac{A^m}{12}\begin{bmatrix}2 & 1 & 1\\ & 2 & 1\\ & & 2\end{bmatrix}$ |
| [B3000S] | $\int_{R_m} \{\phi\}\{\phi\}\{\phi\}^T d\tau$ | $\frac{A^m}{60}\begin{bmatrix}\begin{Bmatrix}6\\2\\2\end{Bmatrix} & \begin{Bmatrix}2\\2\\1\end{Bmatrix} & \begin{Bmatrix}2\\1\\2\end{Bmatrix}\\ & \begin{Bmatrix}2\\6\\2\end{Bmatrix} & \begin{Bmatrix}1\\2\\2\end{Bmatrix}\\ & & \begin{Bmatrix}2\\2\\6\end{Bmatrix}\end{bmatrix}$ |
| {B11} | $\{\phi\}_{,k}$ | $\hat{c}_2 \cdot \begin{Bmatrix}\phi_1\\\phi_2\\\phi_3\end{Bmatrix}_{,2} + \hat{c}_3 \cdot \begin{Bmatrix}\phi_1\\\phi_2\\\phi_3\end{Bmatrix}_{,3}$ |
| [A200S] | $\int_{\partial R_m} \{\phi\}\{\phi\}^T d\sigma$ | $\frac{\ell^m}{6}\begin{bmatrix}2 & 1\\ & 2\end{bmatrix}$ |
| {A10} | $\int_{\partial R_m} \{\phi\} d\sigma$ | $\frac{\ell^m}{2}\begin{Bmatrix}1\\1\end{Bmatrix}$ |

(1) Matrix names are a 6 digit code covering dimensionality, nonlinearity, degree of differentiation and special matrix properties, as [a, b, c, d, e, f] where:
a = A, B, C for spaces of one-, two-, and three-dimensions,
b = number of coordinate functions appearing in integral or matrix,
c, d, e = (0,1) Boolean counters indicating (no, yes) differentiation of each function,
e or f = S, A, Δ for matrix symmetric, antisymmetric or general.

(2) Symmetric matrices are written in upper triangular form.

(3) $A^m$ = 1/2 (X2P2)(X3P3), the plane area of the triangular finite element.
X2P2 = the $x_2$ prime coordinate of node 2,
X3P3 = the $x_3$ prime coordinate of node 3.

(4) $\ell^m$ = length of side for boundary condition (=X2P2).

$$\{L\}_{,k} = \frac{1}{x_2}\begin{Bmatrix} -1 \\ 1 \\ 0 \end{Bmatrix}\hat{i} + \frac{1}{x_2 y_3}\begin{Bmatrix} x_3 - x_2 \\ -x_3 \\ +x_2 \end{Bmatrix}\hat{j} \qquad \text{B-8}$$

where $\hat{i}$ and $\hat{j}$ are unit vectors in the local reference system.

Integration of polynomials over domains, which is required to obtain the finite element formulation of the partial differential equations is straightforward using the integration formula shown in Table B-3. A series of reoccurring integral expressions is presented and identified in Table B-4.

The computations are related to the physical conical system consisting of an annular conical ring normal to the surface of the cone. The conical coordinate system and the physical annular surface are shown in Figure 3-7b. This figure also identifies the mesh system and finite elements over which the expressions are evaluated. The curvilinear coordinates are characterized by the shape factors $h_1$, $h_2$, and $h_3$ which, of course, are evaluated in the physical conical system. For computational purposes by finite element method, the annular conical element is reduced to a rectangular global system with $x_2$ and $x_3$ coordinates in the discretization plane and the streamwise coordinate $x_1$ normal to it. The relation between the local and global coordinate system is shown in Figures 3-7b and B-1. Form the weighted residual of Equation B-1 by substitution and integration over $R_m$, after premultiplication by $\{L\}$, to yield:

$$\int_{R_m} \{L\}N(q^*)d\tau + \lambda\int_{\partial R_m} \{L\}B(q^*)d\sigma \equiv 0 \qquad \text{B-9}$$

After (a) formation of Equation B-9 for every element $R_m$, (b) Boolean assembly of these M equations, (c) integration by parts of the generalized elliptic operator term, and (d) identification of the Lagrange multiplier, $\lambda$, with the Reynolds, Prandtl, or

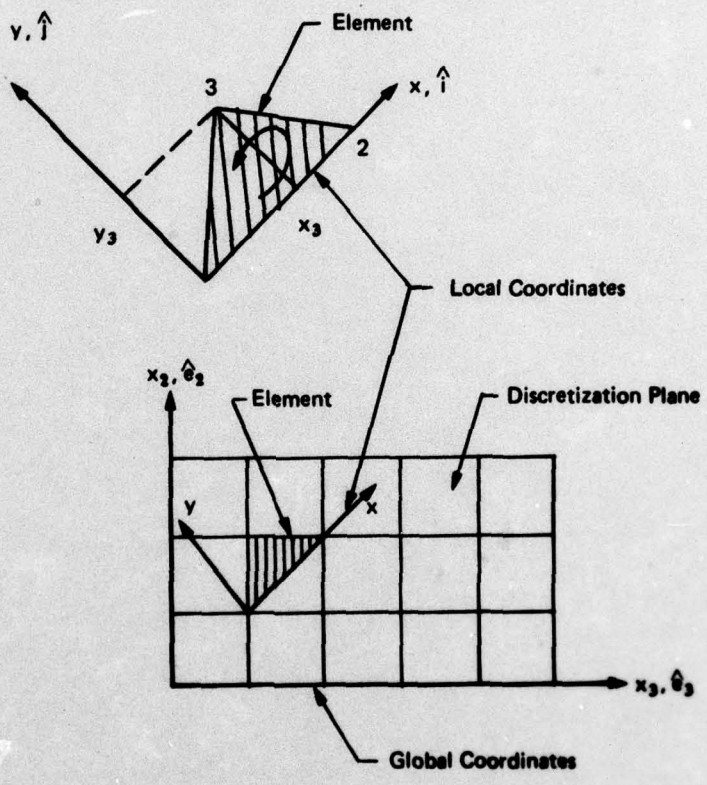


Figure B-1. Global and Local Coordinate Systems

Schmidt numbers, as appropriate, the global finite element solution algorithm is established. The resultant equation system is first-order, ordinary differential and is written on the $x_1$ behavior of the elements of {Q}, the global discretized dependent variable vector. It can be rendered in the standard form:

$$\left[Q\right]' = f(\left[Q\right], x_1) \qquad \text{B-10}$$

and solved for Q using an integration algorithm.

Considering the $x_1$ momentum equation:

$$L(u) = \rho(u_{,t} + u_j u_{1,j}) - \frac{1}{Re}(\tau_{1j})_{,j} + p_{,1} = 0 \qquad \text{B-11}$$

with boundary conditions

$$B(u) = a_1 u + a_2 k u_{,i} n_i - a_3 = 0 \qquad \text{B-12}$$

The method of weighted residuals is applied

$$\int_{R_m} \{L\} L(u) d\tau + \lambda \int_{\partial R_m} \{L\} B(u) d\sigma = 0 \qquad \text{B-13}$$

With the aid of the Green-Gauss theorem and assuming that the viscous streamwise derivatives are small compared with the viscous normal and circumferential derivatives ($\frac{\partial(\ )}{\partial x_1} << \frac{\partial(\ )}{\partial x_2}$, $\frac{\partial(\ )}{\partial x_3}$) and for all velocities of the order $\sigma(1)$ (u, v, w = $\sigma(1)$) one obtains the following form of the $x_1$ momentum equation after applying the method of weighted residuals:

$$\int_{R_m} \{L\}\rho \left[\frac{u}{h_1}\frac{\partial u}{\partial x_1} + \frac{v}{h_2}\frac{\partial u}{\partial x_2} + \frac{w}{h_3}\frac{\partial u}{\partial x_3} + \frac{uv}{h_1 h_2}\frac{\partial h_1}{\partial x_2}\right.$$

$$\left. + \frac{uw}{h_1 h_3}\frac{\partial h_1}{\partial x_3} - \frac{v^2}{h_1 h_2}\frac{\partial h_2}{\partial x_1} - \frac{w^2}{h_1 h_3}\frac{\partial h_3}{\partial x_1}\right] d\tau$$

$$+ \int_{R_m} \{L\}\frac{1}{h_1}\frac{\partial p}{\partial x_1} d\tau - \frac{1}{Re}\int_{R_m}\left[\frac{1}{h_2}\frac{\partial}{\partial x_2}\{L\}\frac{\mu}{h_2}\frac{\partial u}{\partial x_2}\right.$$

$$\left. + \frac{1}{h_3}\frac{\partial}{\partial x_3}\{L\}\frac{\mu}{h_3}\frac{\partial u}{\partial x_3}\right] d\tau$$

$$+ \frac{1}{Re}\int_{\partial R_m} \{L\}\left[\frac{a_1}{a_2}u - \frac{a_3}{a_1}\right] d\sigma = 0 \qquad \text{B-14}$$

Approximating the dependent variable q by a series expansion of the form

$$q_m^*(x_i) = \{L(x_2,x_3)\}^T\{Q(x_1)\}_m \qquad \text{B-15}$$

where the elements of the column matrix $\{Q\}_m$ are the unknown values of q at the nodes of $R_m$, and the elements of $\{L\}$ are known polynomial shape functions (Equation B-7), with

$$u_m^* = \{L\}^T\{u(x_1)\}_m \qquad \text{B-16}$$

$$(\rho u)_m^* = \{L\}^T\{RHOU\}_m \qquad \text{B-17}$$

the first term of the $x_1$-momentum equation becomes after evaluating the integrals (Table B-3):

$$\frac{1}{h_1}\int_{R_m} \{L\}\rho u\frac{\partial u}{\partial x} d\tau = \frac{1}{h_1}\int_{R_m} \{L\}\{L\}^T\{RHOU\}_m\{L\}^T\{u\}\,d\tau$$

$$= \frac{1}{h_1}\frac{A_m}{60}\begin{bmatrix} \{6,2,2\} & \{2,2,1\} & \{2,1,2\} \\ & \{2,6,2\} & \{1,2,2\} \\ & & \{2,2,6\} \end{bmatrix}\{RHOU\}\{u\} \qquad \text{B-18}$$

Evaluating all terms of the $x_1$ momentum equation in a similar way, a first-order ordinary differential equation written for $u(x_1)$ is obtained in the standard form:

$$\left[u\right]' = f(\left[u\right], x_1) \qquad \text{B-19}$$

which can be solved for u at the downstream $x_1$ station using any integrating algorithm. The remaining momentum equations and the energy equation are reduced similarly to finite element form.

The first term of the energy equation, the initial value term, assumes the following finite element form upon integration

$$\int_{R_m} \{\phi\} \frac{\rho u_1}{h_1} \frac{\partial H}{\partial x_1} d\tau = \frac{1}{h_1} \{\rho u\}^T \frac{A_m}{60} \begin{bmatrix} \begin{Bmatrix}6\\2\\2\end{Bmatrix} & \begin{Bmatrix}2\\2\\1\end{Bmatrix} & \begin{Bmatrix}2\\1\\2\end{Bmatrix} \\ & \begin{Bmatrix}2\\6\\2\end{Bmatrix} & \begin{Bmatrix}1\\2\\2\end{Bmatrix} \\ & & \begin{Bmatrix}2\\2\\6\end{Bmatrix} \end{bmatrix} \{H\}' \qquad \text{B-20}$$

Having reduced to the finite element form all terms of the energy equation this way, the downstream value of the dependent variable, the total enthalpy H is evaluated by integration scheme.

This entire system of equations including the continuity equation has been integrated into a single code. Extensive computational exercises of the flow field, including a number of variations of parameters, have been performed. A comprehensive documentation of the pertinent computational results is presented.

## Appendix C

## Solution of Continuity Equation

The continuity equation for a general steady state curvilinear case has the form

$$\frac{\partial}{\partial x_1}(h_2 h_3 \rho u) + \frac{\partial}{\partial x_2}(h_1 h_3 \rho v) + \frac{\partial}{\partial x_3}(h_1 h_2 \rho w) = 0 \qquad \text{C-1}$$

After introducing the finite difference expression, the derivative in the normal direction is given by

$$\frac{\partial}{\partial x_2}(h_1 h_3 \rho v)_{\ell+1} = \left[ \frac{(h_1 h_3 \rho v)^n - (h_1 h_3 \rho v)^{n-1}}{dx_2^{n-1}} \right]_{\ell+1}$$

$$= -\left[ \frac{\partial}{\partial x_1}(h_2 h_3 \rho u) + \frac{\partial}{\partial x_3}(h_1 h_2 \rho w) \right]^n_{\ell+1} \qquad \text{C-2}$$

The desired value of the normal velocity $v^n_{\ell+1}$ at the n station in the normal direction, and at the downstream station ($\ell$+1) is

$$(h_1 h_3 \rho v)^n_{\ell+1} = (h_1 h_3 \rho v)^{n-1}_{\ell+1} - \left[ \frac{\partial}{\partial x_1}(h_2 h_3 \rho u) + \frac{\partial}{\partial x_3}(h_1 h_2 \rho w) \right]^n_{\ell+1} dx_2^{n-1} \qquad \text{C-3}$$

The sum of derivative in the expression [ ] is evaluated appropriately and the normal velocity is determined by the finite difference method in each column marching from the wall toward the edge of the boundary layer.